

Reconstructing the seafloor environment during sapropel formation using benthic foraminiferal trace metals, stable isotopes, and sediment composition

Ní Fhlaithearta, Gert-Jan Reichart, Frans Jorissen, Christophe Fontanier, E.-J. Rohling, J. Thomson, Gert de Lange

▶ **To cite this version:**

Ní Fhlaithearta, Gert-Jan Reichart, Frans Jorissen, Christophe Fontanier, E.-J. Rohling, et al.. Reconstructing the seafloor environment during sapropel formation using benthic foraminiferal trace metals, stable isotopes, and sediment composition. Paleoceanography, 2010, 25 (4), Non spécifié. 10.1029/2009PA001869 . hal-03278050

HAL Id: hal-03278050

https://univ-angers.hal.science/hal-03278050

Submitted on 8 Jul 2021

HAL is a multi-disciplinary open access archive for the deposit and dissemination of scientific research documents, whether they are published or not. The documents may come from teaching and research institutions in France or abroad, or from public or private research centers.

L'archive ouverte pluridisciplinaire **HAL**, est destinée au dépôt et à la diffusion de documents scientifiques de niveau recherche, publiés ou non, émanant des établissements d'enseignement et de recherche français ou étrangers, des laboratoires publics ou privés.

Copyright

Reconstructing the seafloor environment during sapropel formation using benthic foraminiferal trace metals, stable isotopes, and sediment composition

S. Ní Fhlaithearta,[1] G.-J. Reichart,[1,2] F. J. Jorissen,[3,4] C. Fontanier,[3,4] E. J. Rohling,[5] J. Thomson,[5] and G. J. De Lange[1]

Received 5 October 2009; revised 17 June 2010; accepted 30 June 2010; published 11 December 2010.

[1] The evolution of productivity, redox conditions, temperature, and ventilation during the deposition of an Aegean sapropel (S1) is independently constrained using bulk sediment composition and high-resolution single specimen benthic foraminiferal trace metal and stable isotope data. The occurrence of benthic foraminifer, *Hoeglundina elegans (H. elegans)*, through a shallow water (260 m) sapropel, permits for the first time a comparison between dissolved and particulate concentrations of Ba and Mn and the construction of a Mg/Ca–based temperature record through sapropel S1. The simultaneous increase in sedimentary Ba and incorporated Ba in foraminiferal test carbonate, $(Ba/Ca)_{H.\ elegans}$, points to a close coupling between Ba cycling and export productivity. During sapropel deposition, sedimentary Mn content ($(Mn/Al)_{sed}$) is reduced, corresponding to enhanced Mn^{2+} mobilization from sedimentary Mn oxides under suboxic conditions. The consequently elevated dissolved Mn^{2+} concentrations are reflected in enhanced $(Mn/Ca)_{H.\ elegans}$ levels. The magnitude and duration of the sapropel interruption and other short-term cooling events are constrained using Mg/Ca thermometry. Based on integrating productivity and ventilation records with the temperature record, we propose a two-mode hysteresis model for sapropel formation.

Citation: Ní Fhlaithearta, S., G.-J. Reichart, F. J. Jorissen, C. Fontanier, E. J. Rohling, J. Thomson, and G. J. De Lange (2010), Reconstructing the seafloor environment during sapropel formation using benthic foraminiferal trace metals, stable isotopes, and sediment composition, *Paleoceanography*, *25*, PA4225, doi:10.1029/2009PA001869.

1. Introduction

[2] The eastern Mediterranean sedimentary record is characterized by the frequent occurrence of organic rich layers, called sapropels [*Olausson*, 1961; *Kidd et al.*, 1978]. Sapropels are a sedimentological expression of orbitally induced variations in solar insolation; their occurrence is governed by a 21 kyr periodicity that correlates with precession minima [*Rossignol-Strick et al.*, 1982; *Hilgen*, 1991; *Rohling*, 1994]. According to the most recent synthesis, the youngest sapropel (S1) appears to have formed throughout the eastern Mediterranean between 9.8 and 5.7 ^{14}C kyr B.P. (10.8–6.1 calendar kyr B.P.) [*De Lange et al.*, 2008]. Present consensus is that prior to the onset of sapropel formation in SLA9 (~ 9.2 kyr B.P.), continental runoff from the Nile and Northern Borderland rivers intensified (~ 10.5 kyr B.P.), resulting in an increased supply of freshwater [*Casford et al.*, 2002]. Consequently, vertical density gradients in the upper water column steepened, leading to restricted deepwater formation. Enhanced export productivity during sapropel formation may initially have been fuelled by the input of river derived nutrients, and further sustained by enhanced phosphorus recycling and nitrogen fixation [*Olausson*, 1961; *Vergnaud-Grazzini et al.*, 1977; *Cita et al.*, 1977; *Rossignol-Strick et al.*, 1982; *Rohling and Hilgen*, 1991; *Sachs and Repeta*, 1999; *Casford et al.*, 2002; *Rohling et al.*, 2004; *Slomp et al.*, 2004]. Evidence for extensive nitrogen fixation during sapropel conditions invokes oligotrophic surface waters, suggesting that the contribution of river-derived nutrients to surface waters was minor [*Sachs and Repeta*, 1999].

[3] Furthermore *Casford et al.* [2002] presented a case for an initial period of 1000–1500 years of nutrient accumulation prior to the onset of sapropel deposition. This would suggest that the nutrient budget for the actual period of sapropel deposition should not be considered in terms of a steady state process, but that it included nutrients imported into the basin during the extensive early phase of flooding. The process involved would be initial deposition on the shelves/slopes, and subsequent remobilization/recycling during the sapropel event. Increased productivity during sapropel deposition is based on a higher export flux of organic matter, reflected in sediment cores by enhanced organic carbon (C_{org}) and biogenic barium content [*Thomson et al.*, 1995; *van Santvoort et al.*, 1996].

[1]Department of Earth Sciences–Geochemistry, Faculty of Geosciences, Utrecht University, Utrecht, Netherlands.
[2]Alfred-Wegener Institute, Bremerhaven, Germany.
[3]Laboratory of Recent and Fossil Bio-Indicators, UPRES EA 2644, Angers University, Angers, France.
[4]Laboratoire d'Etude des Bio-Indicateurs Marins, Ile d'Yeu, France.
[5]National Oceanography Centre, Southampton, UK.

Copyright 2010 by the American Geophysical Union.
0883-8305/10/2009PA001869

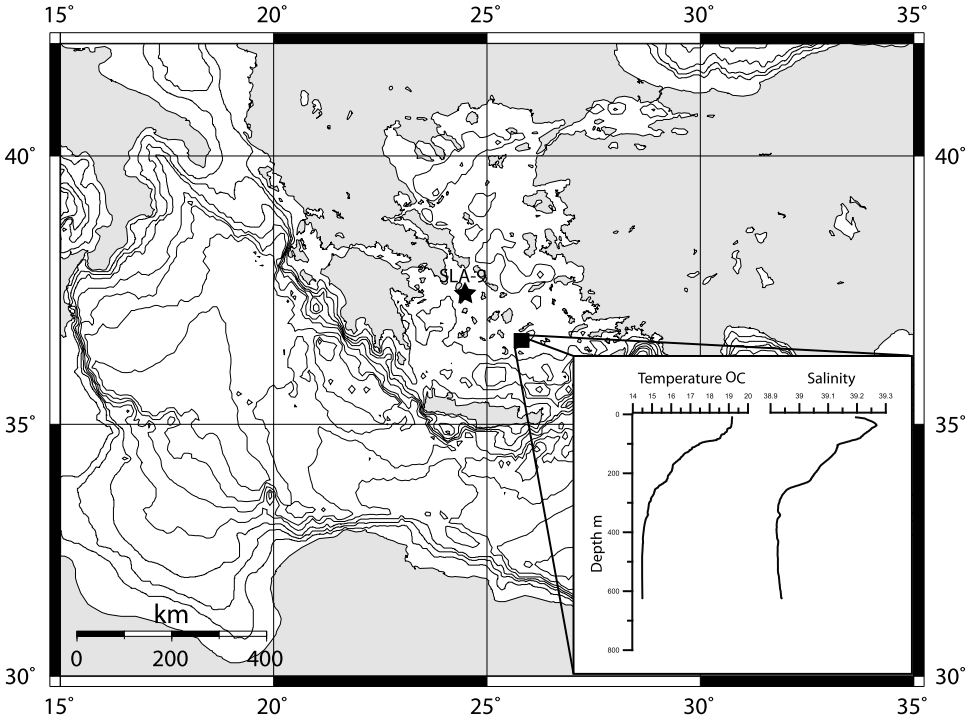


Figure 1. Map of the Aegean showing the location of core SLA-9. Inset temperature and salinity profile from CTD 588, taken during cruise Meteor 51-3 (courtesy of C. Hemleben).

[4] The combination of higher organic matter remineralization [*Passier et al.*, 1996] and decreased ventilation resulted in widespread bottom water anoxia [*Rohling and Gieskes*, 1989; *Rohling*, 1994]. Past anoxia is recognized in sediment cores by an absence of benthic foraminifera, depleted sedimentary Mn concentrations and the presence of reduced mineral species such as pyrite [*Passier et al.*, 1996; *Jorissen*, 1999; *Thomson et al.*, 1999].

[5] Discussions of sapropel formation center on the relative roles of enhanced export production and redox controlled enhanced organic matter preservation, in controlling the organic carbon content of sapropels. Both processes not only interact during sapropel formation, but are also intimately linked in proxy data. More recently, sapropel studies have also focused on a centennial scale interruption in sapropel deposition, recognized in cores throughout the eastern Mediterranean [*Rohling et al.*, 1997; *De Rijk et al.*, 1999]. The sapropel interruption is considered to have resulted from an increase in frequency and intensity of winter cooling, which led to an abrupt collapse of stratification and consequent reoxygenation of bottom waters down to more than 1500 m [*Casford et al.*, 2003] but no deeper than 1800 m [*De Lange et al.*, 2008]. Sapropel formation is thus characterized by the complex interplay of productivity and ventilation, with superimposed impacts from abrupt cooling events. Only by using independent multiproxy records can we hope to deconvolve the resulting complex sedimentary phenomena.

[6] Foraminifera have long been used by paleoclimatologists to unravel past changes in the physical and chemical properties of seawater [*Parker*, 1958; *Ruddiman*, 1971; *Lea and Boyle*, 1989; *Rosenthal et al.*, 1997; *Lear et al.*, 2000; *Rosenthal et al.*, 2006; *Jorissen et al.*, 2007]. Records of variations in trace metals and stable isotopes can be extracted from the carbonate tests of benthic foraminifera. The benthic foraminifer *Hoeglundina elegans* is of particular interest in trace metal investigation. First, it possesses an aragonitic test that is less susceptible to diagenetic overgrowths than the calcitic shells of most other perforate benthic foraminifera [*Boyle et al.*, 1995]. Often, foraminiferal Mn oxide coatings have to be removed from calcitic taxa by elaborate cleaning procedures, which complicates trace metal measurements and may also bias the trace metal record through the preferential removal of the more labile calcium carbonate phases [*Yu et al.*, 2007]. Second, globally, *H. elegans* has a cosmopolitan distribution and lives over a wide range of water depths [*Parker*, 1958; *Lutze and Coulbourn*, 1984; *Boyle et al.*, 1995; *Hughes et al.*, 2000; *Koho et al.*, 2008]. In a study of the Aegean Sea, *Parker* [1958] reports the presence of *H. elegans* within a water depth range of 80–1300 m. *Hoeglundina elegans* preferentially lives at or close to the sediment-water interface [*Jorissen et al.*, 1998; *Schönfeld*, 2001; *Fontanier et al.*, 2002], which is commonly explained in terms of the maximum concentration of labile food particles there [*Jorissen et al.*, 2007], and as such provides a record of the chemistry of oceanic bottom waters and surfi-

cial pore waters [*Boyle et al.*, 1995; *Reichart et al.*, 2003; *Rosenthal et al.*, 2006]. The combination of these characteristics makes it an ideal candidate for tracking variations in bottom water trace metal concentrations through time.

[7] Core SLA-9 was retrieved with R/V *Aegeo* by gravity corer from the Cyclades Plateau (37°31′N, 24°33′E) in the southwestern Aegean Basin, from a depth of 260 m (Figure 1). The water column is characterized by temperatures ranging from 19°C at the surface to 14.5°C at depth (~300 m) and salinity ranging from 39.3 to 38.9 (Figure 1, inset). The Aegean currently plays a key role in eastern Mediterranean circulation as a site of deep and intermediate water formation for the entire eastern Mediterranean basin [*Theocharis*, 1989; *Roether et al.*, 1996; *Lascaratos et al.*, 1999]. The sensitivity of this hydrographic link to cold climatic events [*Roether et al.*, 1996] makes the Aegean a key region for study of the causes of eastern Mediterranean reoxygenation at sapropel interruption and termination [*Casford et al.*, 2003; *Marino et al.*, 2007]. Studying sapropel formation furthers our understanding of the impact of abrupt climate change on circulation and deep water formation in the Mediterranean. Of broader significance, Mediterranean sapropels offer an ideal test bed for detailed studies of the processes governing organic matter burial, and of the sensitivity of thermohaline ventilation processes to climate change.

[8] In this study, the application of laser ablation-ICP-MS (LA-ICP-MS) to benthic foraminifer *H. elegans* provides a new tool in the reconstruction of bottom water conditions during sapropel deposition. Laser ablation-ICP-MS is virtually nondestructive and permits both the repeated analysis of scarce foraminifera and the subsequent measurement of their oxygen and carbon isotope ratios, thus avoiding any potential offsets between individuals. By coupling the dissolved Ba and Mn records, as deduced from *H. elegans*, with their solid phase counterparts, we potentially gain new insights into surface water productivity, biogenic barium preservation, and the evolution of redox conditions throughout the sapropel. We use Mg/Ca thermometry to constrain the duration and magnitude of the cooling during the sapropel interruption. Other centennial scale cooling events, previously suggested by changes in planktonic and benthic foraminiferal assemblage changes [*De Rijk et al.*, 1999; *Rohling et al.*, 2002; *Abu-Zied et al.*, 2008], close to the onset and termination of sapropel S1, are similarly constrained. The uninterrupted presence of *H. elegans* in SLA-9 [*Abu-Zied et al.*, 2008] combined with LA-ICP-MS, thus presents a unique opportunity to better characterize the key forcing mechanisms for environmental change in the Aegean [*Casford et al.*, 2003] and the deep eastern Mediterranean.

2. Materials and Methods

[9] Core SLA-9 was sampled using U channels that were subsampled in a continuous series of 0.5 cm intervals for faunal analysis, and 1 cm intervals for bulk sediment analysis.

[10] For bulk sediment analysis a subsample was freeze-dried and thoroughly ground in an agate mortar. The powder was digested in a mixture of HF, HNO_3 and $HClO_4$, evaporated to near dryness, before being taken up again in a solution of 1M HCl. Solutions were measured by inductively coupled plasma–optical emission spectroscopy (ICP-OES) (Perkin Elmer Optima 4300DV), with an instrumental precision of better than 3%, for the elements reported. Dilution effects due to varying input rates of carbonate and detrital material are eliminated by normalizing sediment elemental concentrations against Al.

[11] Another part of each subsample was used for foraminiferal preparation, for abundance counts, stable isotopes, shell chemistry, and AMS radiocarbon dating. These aliquots were first dried at 50° for 24–48 h, after which they were wet sieved with distilled water and separated into 600, 150, 125 and 63 μm fractions.

[12] For shell chemistry, we picked the aragonitic benthic foraminiferal species *H. elegans* from the > 150 μm fraction. The trace metal composition of *H. elegans* was measured by laser ablation using a deep UV (193 nm) excimer laser (Lambda Physik) with GeoLas 200Q optics. Ablation was performed at a pulse repetition rate of 5 Hz, an energy density of 10 J/cm^2, and a crater size of 20 μm. Ablated particles were measured by a quadrupole ICP-MS (Micromass Platform). Calibration was performed against international glass standard (NIST612), using the *Pearce et al.* [1997] concentration data and ^{44}Ca as an internal standard, while monitoring the ^{42}Ca and ^{43}Ca minor isotopes. Using a 193 nm wavelength for ablating glass standard and calcite tests minimizes matrix effects [*Hathorne et al.*, 2008]. Isotopes used for element quantification were ^{24}Mg, ^{27}Al, ^{55}Mn, ^{138}Ba and ^{208}Pb. All *H. elegans* specimens were ablated twice on their umbilical side. Analytical error (equivalent to 1 sigma), based on the repeated measurement of an external standard, was ± 8% for Ba, ± 8% for Mn, ± 10% for Mg and ± 6% for Sr. Each laser ablation measurement was screened for contamination and diagenetic coatings by monitoring Al, Mn and Pb. On encountering surficial clay contamination (indicated by Al peak) the data integration interval was adjusted to exclude the Al enrichment (see Figure 2). Based on laser ablation profiles, there was no indication of diagenetic Mn coatings on this sample set. As each laser ablation pulse removes approximately 50 nm per pulse, even microscopic coatings of Mn oxides would be detected by this method. Data from single specimen trace metal analyses are prone to scatter due to inter and intraspecimen variations [*Sadekov et al.*, 2005], possibly related to microhabitat and/or vital effects (see Tables A1–A3). We applied a 500 year moving Gaussian window to the benthic foraminiferal trace metal and stable isotope data in order to highlight robust trends.

[13] Analyses of stable oxygen and carbon isotope ratios based on single specimens of *H. elegans* ($\delta^{18}O_{H.\ elegans}$ and $\delta^{13}C_{H.\ elegans}$) were performed at Utrecht University using an automated individual acid bath carbonate preparation device (KIEL III), coupled to a dual-inlet isotope ratio mass spectrometer (Finnigan MAT253). The results were calibrated using an international (NBS-19) and an in-house standard. Precision (1 sigma), based on external standards, is within 0.05‰ and 0.08‰ for $\delta^{13}C$ and $\delta^{18}O$, respectively. Results are reported in ‰ relative to the Vienna Pee Dee Belemnite (V-PDB) standard.

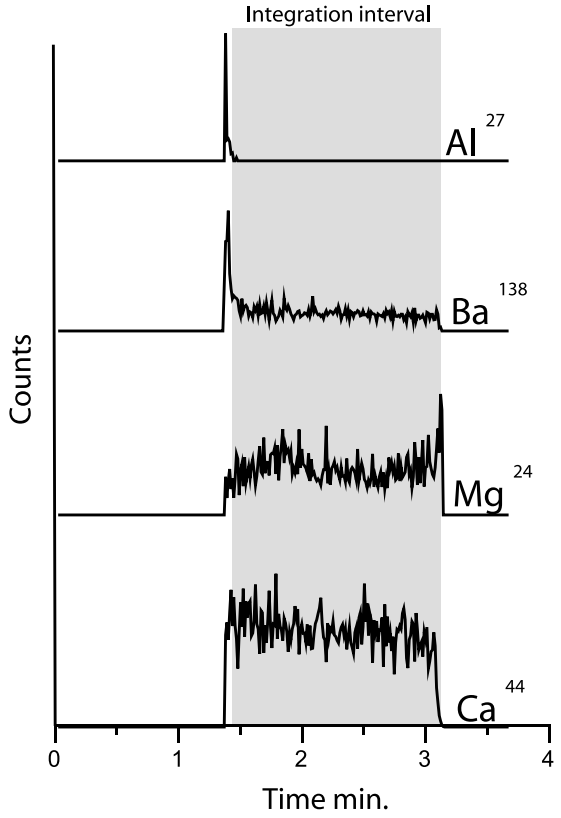


Figure 2. Example of a laser ablation profile measured in counts per time showing how data integration window (gray shading) is adjusted to include only data unaffected by Al contamination.

[14] Atomic mass spectrometry radiocarbon datings and the age model for SLA-9 have been previously described by *Casford et al.* [2002, 2007] and *Abu-Zied et al.* [2008]. All dates presented here are given in conventional ^{14}C years. Stable O and C isotope results for the surface-dwelling planktonic foraminiferal species *Globigerinoides ruber* (white) have been previously described by *Casford et al.* [2002].

3. Results

[15] The sapropel interval is characterized by dark olive gray sediments extending from 103 to 84 cm depth, (9000 years B.P. and 7900 years B.P.) followed by light gray muds up to 64 cm (6100 years B.P.) (Figures 3 and 4a). Downward from the sapropel, a continuous transition is observed to light gray sediments, which continue down to about 113 cm depth (10,600 years B.P.).

[16] In core SLA-9, $(Ba/Al)_{sed}$ ratios show a first peak at 9650 years B.P., followed by a sharp drop at 9350 years B.P. (Figure 4d). Immediately thereafter, at 9200 years B.P., $(Ba/Al)_{sed}$ ratios abruptly increase to maximum values, which are attained at 8900 years B.P. Subsequently $(Ba/Al)_{sed}$ ratios remain high until a strong drop starting at about 6350 years B.P. Holocene background levels are reached at 6100 years B.P. Thus the extent of the sapropel from initial onset to termination is between 9200 to 6100 years B.P.

[17] The record of low-oxygen tolerant benthic foraminifera for SLA-9 shows an initial increase at around 10250 years B.P. (Figure 4b) [*Casford et al.*, 2003]. They attain a first peak at 9650 years B.P., exactly coincident with the first $(Ba/Al)_{sed}$ peak. After a drop to lower values, the percentage of low-oxygen tolerant benthic foraminifera abruptly increases to maximum values at 9000 years B.P. Values remain high until 6400 years B.P., when their percentage sharply decreases until background levels are reached at about 6100 years B.P. The relative abundance of *H. elegans* is generally < 2% throughout the core. Although such low abundances are difficult to quantify because of counting statistics (the entire 150–600 μm fraction has been used without any partitioning or splitting, in order to pick up to 250 specimens from each sample, or as many as present [*Abu-Zied et al.*, 2008]; however, within the sapropel sometimes only 80 to 150 specimen were present), concentrations do decrease somewhat during the sapropel (Figure 4b).

[18] The $(Ba/Ca)_{H.\ elegans}$ ratios are stable from the bottom of the core to about 9800 years B.P. From there on they increase until a maximum of about 13 μmol/mol at 8300 years B.P. (Figure 4e). After this, values decrease to a minimum at 7400 years B.P., followed by a second interval with high values from 7300 to 6600 years B.P. After this, values fall back to presapropel ratios.

[19] The $(Mn/Al)_{sed}$ values before and after the sapropel are between 12 and 14 mg/g (Figure 4f). A gradual decrease in $(Mn/Al)_{sed}$ starts at the base of the sapropel, culminating

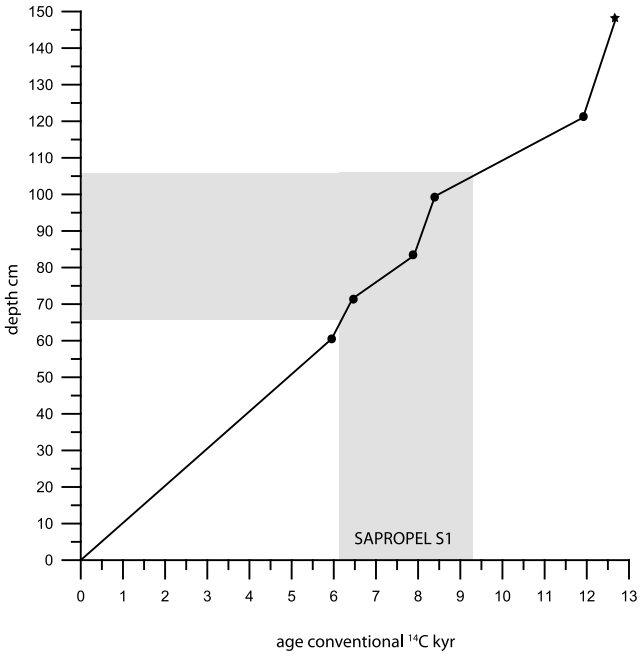


Figure 3. Age-depth plot for core SLA-9. Black circles indicate ^{14}C measurements; black star indicates planktonic foraminiferal assemblage shift (for details, see *Casford et al.* [2002]).

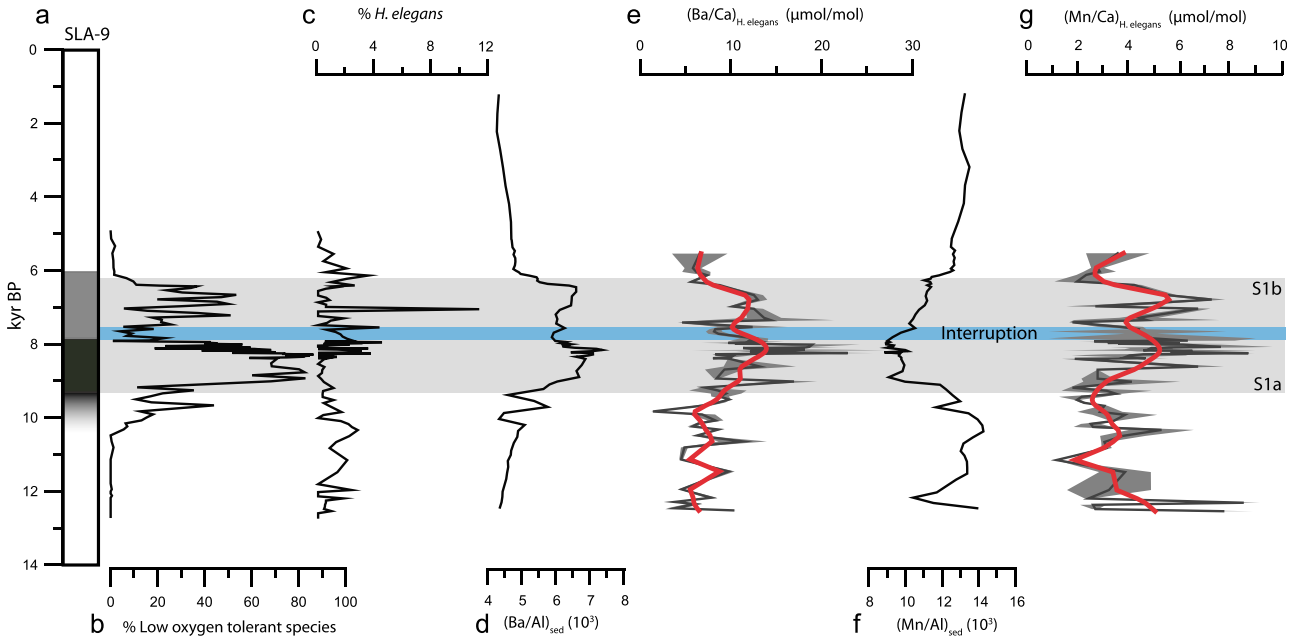


Figure 4. (a) Color description based on core log. (b) Percentage low oxygen tolerant benthic foraminifera assemblages [from *Casford et al.*, 2003]. (c) *Hoeglundina elegans* as percent of total benthic foraminifera assemblage. (d) Elemental ratios versus conventional ^{14}C kyr of sedimentary $(Ba/Al)_{sed}$ [*Casford et al.*, 2007]. (e) Benthic foraminiferal $(Ba/Ca)_{H.\ elegans}$ from core SLA-9. Dark gray line represents $(Ba/Ca)_{H.\ elegans}$ data with standard deviations in gray envelope. Red line represents 500 year Gaussian smoothing of $(Ba/Ca)_{H.\ elegans}$ data. (f) Elemental ratios versus conventional ^{14}C kyr of sedimentary $(Mn/Al)_{sed}$. (g) Benthic foraminiferal $(Mn/Ca)_{H.\ elegans}$ from core SLA-9. Dark gray line represents $(Mn/Ca)_{H.\ elegans}$ data with standard deviations in gray envelope. Red line represents 500 year Gaussian smoothing of $(Mn/Ca)_{H.\ elegans}$ data. Extents of sapropel and sapropel interruption are indicated by gray and blue shading, respectively.

in a minimum of ~9 mg/g at about 8200 years B.P. From this point on we observe a gradual increase until about 6300 years B.P., where values abruptly increase to Holocene "baseline values."

[20] The $(Mn/Ca)_{H.elegans}$ ratios are low throughout our record (Figure 4g). They exhibit a large scatter and the pattern differs distinctly from the sedimentary $(Mn/Al)_{sed}$ ratio. A clear increase can be observed at about 8500 years B.P. Values remain high until 6700 years B.P. with the exception of a drop culminating at 7400 years B.P. After 6700 years B.P. values drop to a new minimum of 2.5 μmol/mol, at 6300 years B.P. Toward the top of the record, values show a slight increase.

[21] Oxygen isotopic values of *H. elegans* display considerable scatter until 10,000 years B.P., followed by less variable, rather heavy, values in the younger part of the record. The offset between $\delta^{18}O_{H.\ elegans}$ and $\delta^{18}O_{G\ ruber}$ is reduced before 12,000 years B.P., but shows no clear systematic variations later in the record (Figure 5).

[22] Throughout the record $\delta^{13}C_{H.\ elegans}$ is heavier than $\delta^{13}C_{G.ruber}$ (Figure 6). Also, there is more scatter in the *H. elegans* record (single-specimen analyses) than in the *G. ruber* record (multiple-specimen analyses), likely related to smoothing effect inherent to multiple-specimen analyses. Overall, $\delta^{13}C_{H.\ elegans}$ shows the same trend to the $\delta^{13}C_{G.\ ruber}$ trend: a gradual decrease toward the sapropel, culminating in a minimum at around 7100 years B.P. A more pronounced step toward lighter values is observed in $\delta^{13}C_{H.\ elegans}$ at about 9000 years B.P. This more abrupt step in $\delta^{13}C_{H.\ elegans}$ causes the isotopic offset between the two species to decrease from this point onward.

[23] The $(Mg/Ca)_{H.\ elegans}$–temperature calibration, adapted from *Reichart et al.* [2003], is best described by an exponential curve ($y = 0.3894e^{0.1564x}$) whereby temperature explains 80% of the variation in $(Mg/Ca)_{H.\ elegans}$ (Figure 7a). The $(Mg/Ca)_{H.\ elegans}$ ratios in SLA-9 fluctuate between 2 and 3.5 mmol/mol (Figure 7b). From 12,500 to 7000 years B.P., values increase from 2.6 to 3.5 mmol/mol. The upper part of the record is interrupted by 3 distinct centennial-scale minima, at 9700 years B.P., 7600 years B.P., and 6000 years B.P. (Figure 7b (A–C)). After 6000 years B.P., values are about 2.9 mmol/mol. From 12,500 years B.P. to 7000 years B.P. the resulting $(Mg/Ca)_{H.\ elegans}$ derived temperature record (Figure 7c) shows a gradual, temperature rise from ~12 to 14°C. Disrupting this general increase in temperature are 3 prominent (~3–4°C) cooling events at 9700 years B.P., 7600 years B.P., and 6000 years B.P. (Figures 7b and 7c (A–C)). However, cooling event A, at 9700 years B.P., is

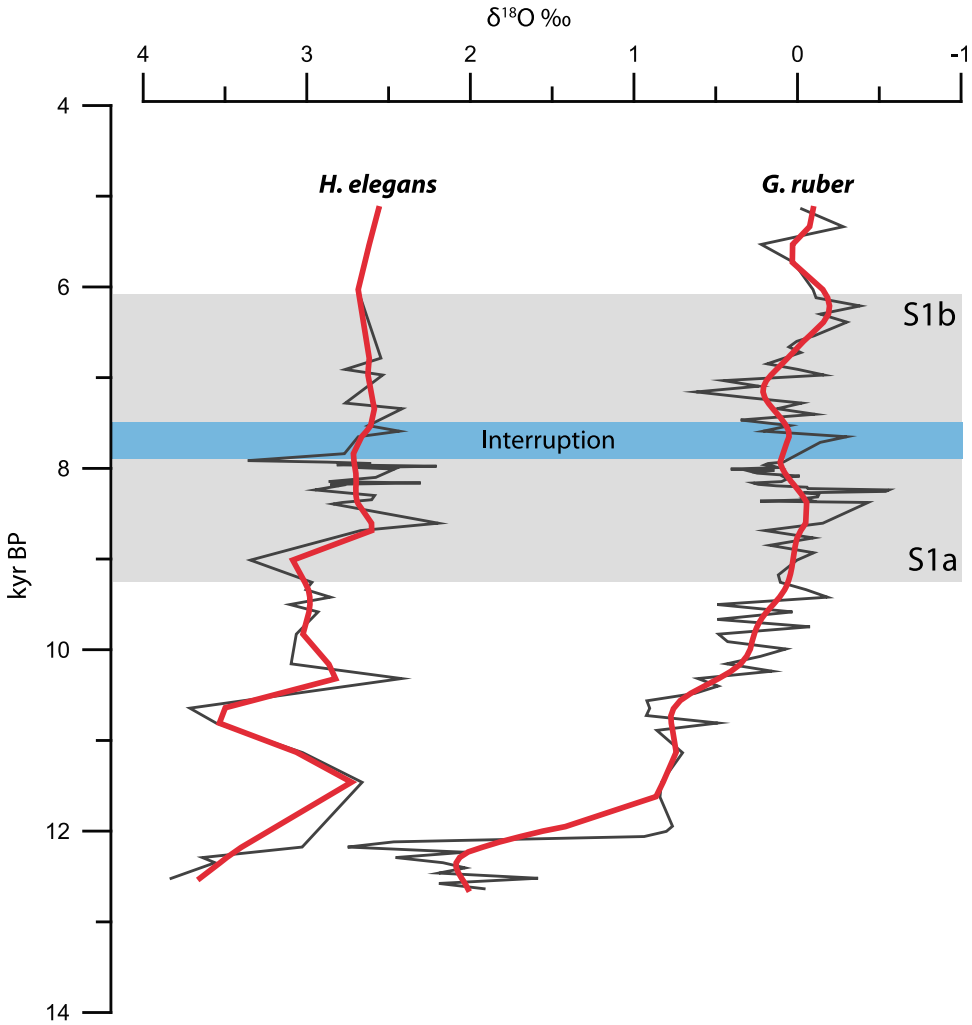


Figure 5. Oxygen isotope records ‰ of *H. elegans* and *G. ruber* [*Casford et al.*, 2002] versus conventional ^{14}C kyr in core SLA-9. Dark gray lines represent data, overlain with red line representing a 500 year Gaussian smoothing. Sapropel and sapropel interruption are indicated by gray and blue shading, respectively.

defined by a single data point. After about 6000 years B.P., $(Mg/Ca)_{H.\ elegans}$ ratios sharply increase again, returning to about 13°C at 5500 years B.P. The *Rosenthal et al.* [2006] $(Mg/Ca)_{H.\ elegans}$–temperature calibration would suggest unrealistically high temperatures (in the order of 50°C). The reason for this discrepancy is unclear. Possibly, given that different analytical methods were employed, the leaching phase in classical foraminiferal trace metal analyses preferentially removed a high Mg phase [*Lohmann*, 1995; *Barker et al.*, 2003] from the more soluble aragonitic shells.

4. Discussion

4.1. *Hoeglundina elegans* as a Recorder of Bottom Water Conditions During Sapropel Formation

[24] In the Atlantic Ocean, *H. elegans* is a low to mid bathyal taxon that seems to prefer oligotrophic, oxic conditions [*Fontanier et al.*, 2002]. However, the species is also known to be able to tolerate low-oxygen environments, such as the California borderland basins [*Douglas and Heitman*, 1979; *Mackensen and Douglas*, 1989]. Because of the extreme oligotrophy that characterizes the eastern Mediterranean [*Antoine et al.*, 1995], *H. elegans* can be found at much shallower water depths, similar to other oligotrophic species [*De Rijk et al.*, 2000]. However, its low percentages in our core suggest that conditions were close to the tolerance limits of the taxon (Figure 4c), and that the depth of the core location is close to the upper bathymetric limit of this species in the southern Aegean Sea.

[25] Due to the low abundances, only few specimens are available for geochemical analysis per sample. Particular care must therefore be taken to ensure that these scarce specimens are autochthonous. Several arguments converge to show that our *H. elegans* specimens are indeed autochthonous: First,

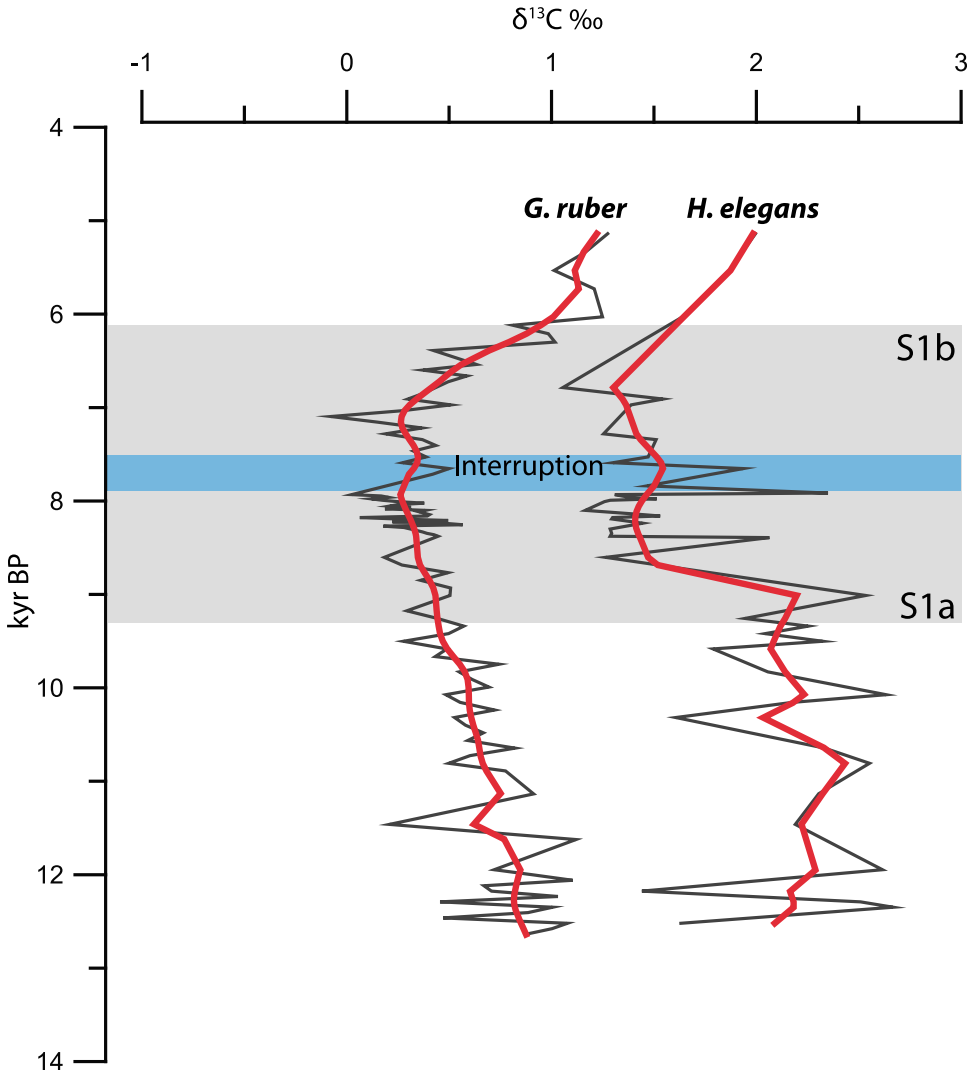


Figure 6. Carbon isotope records ‰ of *H. elegans* and *G. ruber* [*Casford et al.*, 2002] versus conventional ^{14}C kyr in core SLA-9. Dark gray lines represent data, overlain with red line representing a 500 year Gaussian smoothing. Sapropel and sapropel interruption are indicated by gray and blue shading, respectively.

$(Ba/Ca)_{H.\ elegans}$ and $(Mn/Ca)_{H.\ elegans}$ both increase during the sapropel (Figures 4e and 4g), in line with autochthonous *H. elegans* recorded bottom water chemistry during a period of enhanced export flux and/or reduced ventilation. Second, the stepped depletion in $\delta^{13}C_{H.\ elegans}$ at the sapropel onset, and its return to higher values at the sapropel termination, agree with records of other, more abundant benthic foraminifera from core SLA-9 [*Casford et al.*, 2003]. Next, the water depth of 260 m appears to be close to the upper depth limit of *H. elegans* in the Aegean Sea [*Parker*, 1958] so that reworking from shallower sites would be an unlikely source of *H. elegans* specimens. In general, the percentage of displaced epiphytic and other shallow water taxa is very low in our core, and becomes minimal during the deposition of sapropel S1 [*Abu-Zied et al.*, 2008, Figure 9]. Finally, although reworking of older, glacial outcrops could also explain the presence of *H. elegans* in our samples, this is ruled out by the following observations: taxa typical of pre-Holocene conditions, such as *Cibicidoides pachydermus*, *Siphotextularia* spp. and *Trifarina angulosa*, are abundant in the pre-Holocene faunas at the bottom of the core [*Abu-Zied et al.*, 2008]. In sapropel S1, however, these taxa are present only in trace amounts. Thus, it can be excluded that they have been transported from better oxygenated niches in shallower water, or from reworking of older deposits. All these arguments converge to the conclusion that the occurrence of *H. elegans* is the result of a continuous presence of this taxon at the core locality.

[26] Based on benthic foraminiferal studies of nearby cores, we suspect that the locality of SLA-9 (present water

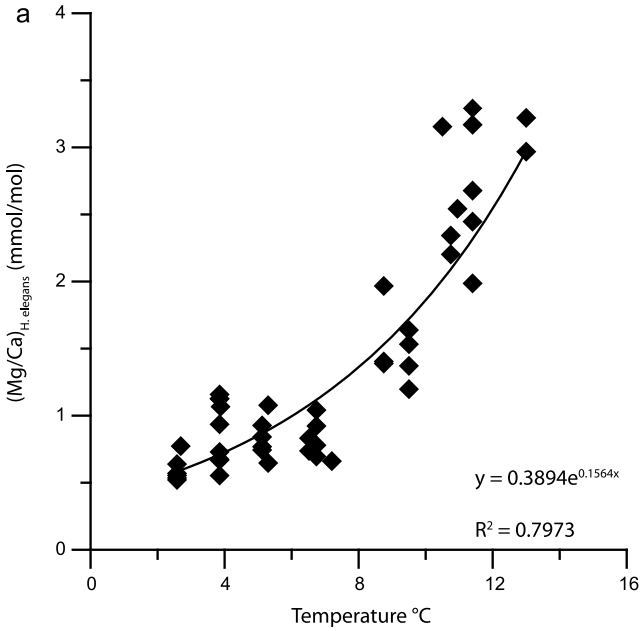


Figure 7. (a) $(Mg/Ca)_{H.\ elegans}$ versus temperature calibration for *H. elegans*, adapted from *Reichart et al.* [2003]. (b) $(Mg/Ca)_{H.\ elegans}$ versus conventional ^{14}C kyr in core SLA-9. Dark gray lines represent $(Mg/Ca)_{H.\ elegans}$ with standard deviations in gray envelope. Red line represents 500 year Gaussian smoothing of underlying data. Cooling events are indicated with letters A–C. Sapropel and sapropel interruption are indicated by gray and blue shading, respectively. (c) Temperature in °C as derived from the $(Mg/Ca)_{H.\ elegans}$ calibration versus kyr B.P. for core SLA-9.

depth 260 m) was positioned several hundreds of meters above the limit of persistently anoxic waters during sapropel times. In fact, also core SL-31 from 430 m depth [*Abu-Zied et al.*, 2008] contains benthic foraminifera throughout, whereas southern Aegean cores GeoTü SL123 from 728 m [*Kuhnt et al.*, 2007] and C40 from 852 m depth [*Geraga et al.*, 2000] were almost devoid of benthic foraminifera during S1 times. These observations suggest that the limit between oxic and persistently anoxic bottom waters was positioned roughly between 500 and 700 m depth. Core SLA-9 not only shows a continuous presence of benthic foraminifera, but it also shows a continuous presence of low quantities of sediment-surface dwelling taxa, which are usually considered sensitive to low oxygen concentrations (e.g., *H. elegans, Gyroidina* spp.), suggesting that the seafloor at our core locality never became continually anoxic.

4.2. Productivity in the Aegean During Sapropel Deposition

[27] Enhanced $(Ba/Al)_{sed}$ ratios indicate that more barium was reaching the seafloor during sapropel formation. Marine sediments contain Ba mainly in the form of biogenic barite ($BaSO_4$) [*Dehairs et al.*, 1980]. Biogenic barite forms as microcrystals in decaying organic debris, a process that underpins its use as a proxy for past productivity in Mediterranean waters [*Bishop*, 1988; *Dymond et al.*, 1996]. Enhanced barite burial fluxes are a function of both productivity and preservation [*Dymond et al.*, 1996]. On reaching the seafloor, $BaSO_4$ partially dissolves in undersaturated bottom waters [*Schenau et al.*, 2001]. The associated release of dissolved Ba to the bottom waters is reflected in enhanced $(Ba/Ca)_{H.\ elegans}$. The degree of dissolution (and thus preservation of $BaSO_4$) depends on the concentration of sulfate and free Ba^{2+} [*Church and Wolgemuth*, 1972] both of which may be slightly modulated with changes in salinity [*Millero and Schreiber*, 1982]. However, a salinity drop of 1–1.5, equivalent to the drop in salinity associated with increased freshwater runoff during sapropel formation [*Rohling*, 1994; *Rohling*, 1999; *Kuhnt et al.*, 2007], results in only an ~1% increase in free Ba^{2+} concentration due to reduced complexation, and a decrease in $BaSO_4$ precipitation by 4% at most. Clearly this is irrelevant in comparison to the observed changes. Alternatively, enhanced $(Ba/Ca)_{H.\ elegans}$ could be related to reduced bottom water ventilation, leading to a build up of deeper water Ba^{2+}. Riverine input during sapropel formation may also serve as an additional local source of Ba^{2+} to the Aegean, as river water is enriched in Ba^{2+} relative to surface waters [*Martin and Meybeck*, 1979; *Hall and Chan*, 2004; *Weldeab et al.*, 2007]. However, this influence is deemed negligible in view of the core location in the southern Aegean being remote from any potential river system. Transport of riverine Ba^{2+} is limited because seawater is at or close to saturation with respect to barite. Finally, barium can be scavenged from seawater by adsorption onto Mn oxides [*De Lange et al.*, 1990], thus remobilization of Mn oxides could result in release of Ba^{2+}. The potential amount of adsorbed Ba that could be released from Mn oxides mobilized during S1 formation is negligible [*Reitz et al.*, 2006], whereas that associated with post S1 Mn oxide formation remain fixed during oxygenated conditions. While $(Ba/Ca)_{H.\ elegans}$ ratios and thus bottom water Ba^{2+} undergo a doubling during sapropel formation, their absolute values still remain relatively low and are comparable to intermediate water values in the north Atlantic [*Reichart et al.*, 2003], which suggests that barite remains undersaturated. Such low values exclude a substantial impact of increased bottom water Ba^{2+} concentrations on sedimentary $BaSO_4$ preservation. In summary, $(Ba/Al)_{sed}$ indicates higher export fluxes, whereas enhanced $(Ba/Ca)_{H.\ elegans}$ during sapropel formation can be attributed to a combination of higher export fluxes and low rates of bottom water ventilation.

4.3. Bottom Water Redox Conditions

[28] Manganese is a redox sensitive element, which is remobilized from solid phase Mn oxide to dissolved Mn^{2+} during oxygen depleted (suboxic) [*Libes*, 2009; *Burdige*, 2006] bottom/pore water conditions [*Froelich et al.*, 1979]. Under such conditions, sedimentary Mn ($(Mn/Al)_{sed}$) becomes depleted as Mn^{2+} is released to the bottom waters. *Hoeglundina elegans*, living at the sediment water interface, will record this increased bottom water Mn^{2+} within its test ($(Mn/Ca)_{H.\ elegans}$) [*Reichart et al.*, 2003; *Boyle*,

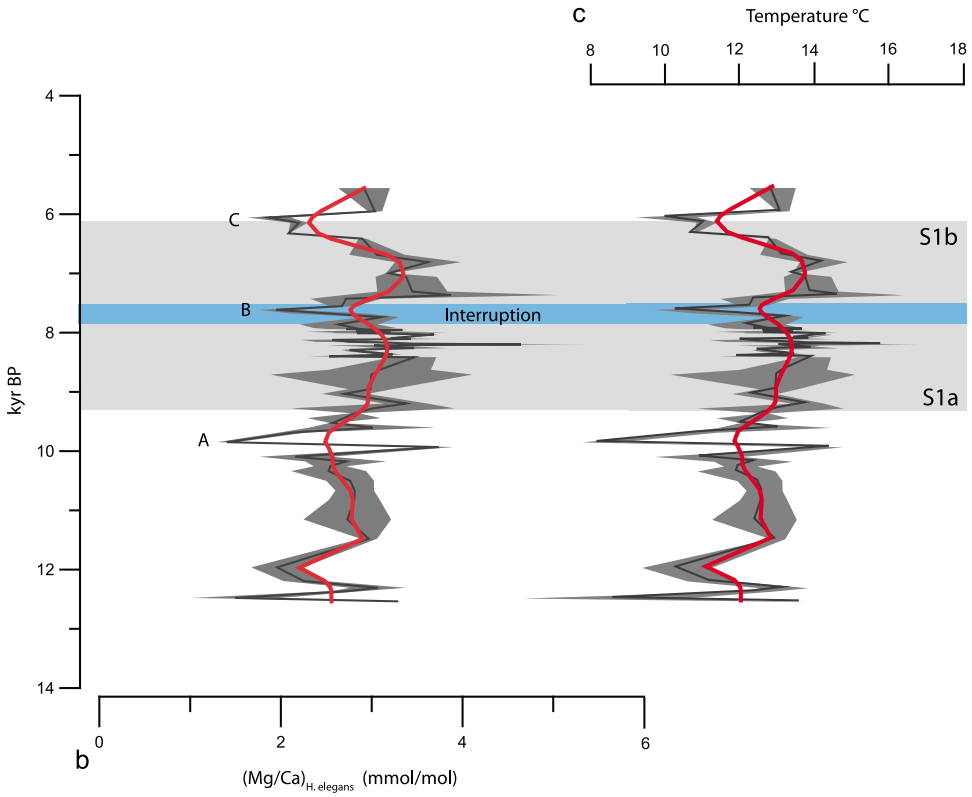


Figure 7. (continued)

1983]. The observed anticorrelation in our record between $(Mn/Ca)_{H.\ elegans}$ and $(Mn/Al)_{sed}$ therefore suggests such enhanced Mn mobilization due to suboxic conditions at or close to the sediment water interface. The high variability seen in $(Mn/Ca)_{H.\ elegans}$ during the sapropel probably primarily reflects the highly dynamic nature of Mn cycling at the sediment water interface.

[29] Using variations in $(Mn/Al)_{sed}$ and $(Mn/Ca)_{H.\ elegans}$ profiles as a framework, we propose a five-step evolution of redox conditions in the southern Aegean during sapropel formation, resulting from the interplay of stratification and water mass isolation with ventilation and reoxygenation. Redox changes may also be driven by higher fluxes of organic matter reaching the seafloor. Increased river runoff during sapropel deposition indeed brought with it a higher flux of riverine organic matter to the Aegean [*Aksu et al.*, 1999]. However, its contribution to redox variations at the sediment water interface would be minor due to its refractive nature [*Burdige*, 2005].

[30] First (10,300 years B.P. to 9000 years B.P.), a gradual decrease in $(Mn/Al)_{sed}$ prior to sapropel formation resulted from partial mobilization of Mn oxides within the sediments (Figure 4f). Continuously low $(Mn/Ca)_{H.\ elegans}$ suggests that the liberated Mn^{2+} reprecipitated immediately above or near the sediment-water interface, which indicates that bottom waters remained oxygenated. The shift to lighter $\delta^{18}O$ values in both *H. elegans* and *G. ruber* at ~10,300 years B.P. is here interpreted to signify a gradual freshening of the entire water column (Figure 5). Based on *G. ruber* alone, *Casford et al.* [2002] previously interpreted this shift as a strengthening of the summer thermocline. However, as a similar shift to lighter $\delta^{18}O$ values also occurs in the benthic foraminiferal species *H. elegans*, this suggests that it is not a seasonal surface water signal, but rather points to a year-round change, affected the whole water column.

[31] Second (9000 years B.P. to 7900 years B.P. (sapropel S1a), a quick onset of oxygen depleted conditions in the bottom waters resulted in rapid mobilization of Mn oxides from the sediment and a build up of Mn^{2+} at the sediment-water interface, where *H. elegans* calcifies. The increase in $(Mn/Ca)_{H.\ elegans}$ at 9000 years B.P. coincides with an abrupt shift to lighter values in both $\delta^{18}O_{H.\ elegans}$ and $\delta^{13}C_{H.\ elegans}$ (see Figures 5 and 6). The observed depletion in $\delta^{13}C_{H.\ elegans}$ can be explained by an enhanced organic matter flux and subsequent remineralization, releasing ^{13}C depleted DIC at the sediment water interface.

[32] Third (7900 years B.P. to 7500 years B.P.), reventilation of the water column drove the Mn^{2+}/MnO_2 redox front back into the sediment during the sapropel interruption.

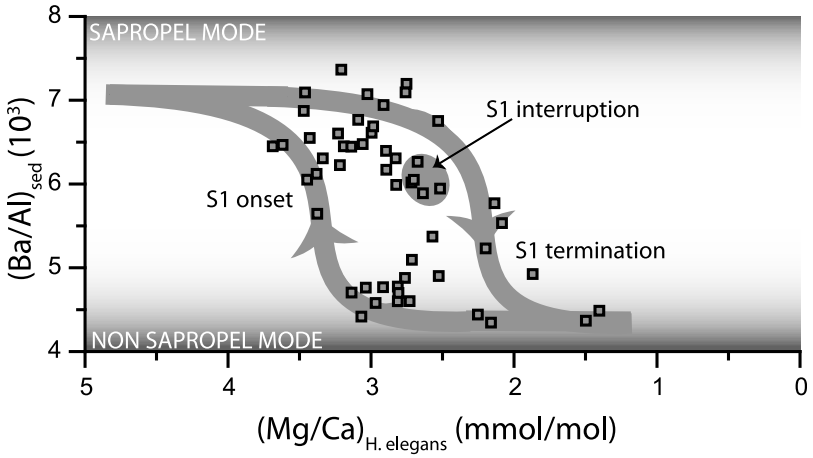


Figure 8. Hysteresis in shifts from nonsapropel to sapropel mode. $(Mg/Ca)_{H.\ elegans}$ (proxy for temperature) is plotted versus $(Ba/Al)_{sed}$ (proxy for organic carbon) to illustrate the two alternate paths between sapropel and nonsapropel conditions.

Consequently $(Mn/Al)_{sed}$ increases, while $(Mn/Ca)_{H.\ elegans}$ decreases (Figures 4f and 4g).

[33] Fourth (7500 years B.P. to 6100 years B.P. (S1b)), reestablishment of suboxic bottom water conditions during the second phase of sapropel deposition led to a renewed migration of the Mn^{2+}/MnO_2 redox front to the sediment water interface, resulting in maximal $(Mn/Ca)_{H.\ elegans}$ values (Figure 4g). Here, $(Mn/Al)_{sed}$ and $(Mn/Ca)_{H.\ elegans}$ no longer exhibit the negative correlation, seen in the previous intervals. Instead $(Mn/Al)_{sed}$ continues to rise gradually until sapropel termination. The absence of expected "low" $(Mn/Al)_{sed}$ values during S1b can be explained as a diagenetic feature due to postdepositional reoxygenation of sediments, or "burn down" whereby a downward diffusing redox front converts Mn^{2+} to Mn oxides, thus obscuring the primary $(Mn/Al)_{sed}$ signal [*van Santvoort et al.*, 1996]. The drop toward Holocene values starts abruptly at 6800 years B.P., where $(Mn/Ca)_{H.\ elegans}$ rapidly decreases as $\delta^{13}C_{H.\ elegans}$ and $\delta^{13}C_{G.\ ruber}$ shift back to heavier values (Figure 6).

[34] Fifth (6100 years B.P. and afterward), complete reventilation of bottom waters at the sapropel termination caused the Mn^{2+}/MnO_2 redox front to migrate back into the sediment. This led to the accumulation of Mn oxides that cause higher $(Mn/Al)_{sed}$ and low $(Mn/Ca)_{H.\ elegans}$.

4.4. Abrupt Centennial-Scale Cooling Events

[35] Abrupt centennial-scale cooling events exert important control on sapropel deposition, as they appear to be responsible for both sapropel interruption and termination (see Figure 7c). Each cooling event (labeled A–C in Figure 7c) results in an approximate drop in temperature of 3–4°C, independently confirming what previous studies, using different methods, have shown [*Rohling et al.*, 1997; *De Rijk et al.*, 1999; *Cacho et al.*, 2001; *Rohling et al.*, 2002]. Cooling event A, though constrained here by a single data point only, may correlate with a short cooling event suggested by planktonic foraminiferal assemblage changes in the Adriatic, at 9500 years B.P. [*Rohling et al.*, 1997; *De Rijk et al.*, 1999]. Cooling events B (sapropel interruption) and C (sapropel termination) have been similarly inferred from regional marine records [*Rohling et al.*, 1997; *De Rijk et al.*, 1999; *Geraga et al.*, 2000; *Mercone et al.*, 2001; *Rohling et al.*, 2002]. These short-term cooling events are attributed to the strengthening and increase in frequency of winter cooling, driven by changes in intensity of high latitude continental air masses [*Theocharis*, 1989; *Roether et al.*, 1996; *Rohling et al.*, 2002].

[36] The 3 cooling events are not evident in either the $\delta^{18}O_{G.\ ruber}$ or the $\delta^{18}O_{H.\ elegans}$ records. The absence of these cooling events in $\delta^{18}O_{G.\ ruber}$ has been suggested by *Rohling et al.* [2002] and *Casford et al.* [2003] to reflect a seasonal offset between climate forcing and the proxy carrier, as cooling is a winter phenomenon and is thus not recorded by *G. ruber*, which thrives in the summer mixed layer [*Rohling et al.*, 1997, 2004]. However, this cannot explain their absence in the $\delta^{18}O_{H.\ elegans}$ record, because subsurface waters derive from wintertime transformation (density increase) of surface waters. We tentatively propose therefore that the cooling events are not observed in the $\delta^{18}O$ records because of a "canceling out" effect. Based on standard oxygen isotope behavior, carbonate formed in fresher waters is more $\delta^{18}O$ depleted and in cool water is more $\delta^{18}O$ enriched. Thus, the simultaneous freshening and cooling of bottom waters during a cooling event would result in a counterbalancing effect on $\delta^{18}O_{H.\ elegans}$. For example, a cooling of maximum 4°C is equivalent to a $\delta^{18}O$ shift of approximately 1‰ [*Epstein et al.*, 1951]. During S1 times, combined stable isotope and salinity modeling suggests that a +1‰ $\delta^{18}O$ effect from temperature reduction might be offset by a ~0.6 salinity reduction [*Rohling*, 1999].

[37] The 9700 years B.P. cooling event occurred 800 years before the sapropel onset. The next cooling event, at about

Table A1. Results of Ba Single Laser Ablation Analyses, With Averages per Test Where Applicable, Standard Deviation, and Standard Error per Depth, Where Applicable[a]

Ablation Code	Depth (cm)	Ba/Ca (μmol/mol)	AVE Test	SD Test	AVE Depth	SD Depth	SE Depth
F2-1	56.25	4.86	4.38	0.67	6.55	3.07	0.72
F2-2	56.25	3.91					
F3-1	56.25	7.39	8.72	1.38			
F3-2	56.25	10.14					
F3-3	56.25	8.62					
F4-1	60.25	5.14	5.80	0.92			
F4-2	60.25	6.45					
F5-2	62.25	5.36	7.28	2.72	6.18	1.56	1.07
F5-3	62.25	9.20					
F6-1	62.25	4.86	5.07	0.31			
F6-2	62.25	5.29					
F8-1	64.25	7.61	7.36	0.36			
F8-3	64.25	7.10					
F9-1	68.25	5.80	5.62	0.26			
F9-2	68.25	8.70					
F9-3	68.25	5.43					
F11-3	70.25	8.84	8.77	0.10			
F11-4	70.25	8.70					
F13-2	73.75	12.54					
F15-1	74.25	12.97					
F17-1	75.75	10.43	10.18	0.36			
F17-2	75.75	9.93					
F18-1	76.25	12.54					
F19-1	78.25	12.32	13.66	1.90			
F19-2	78.25	15.00					
F21-1	78.75	9.78	9.46	0.46	14.40	6.99	1.11
F21-2	78.75	9.13					
F22-1	78.75	17.46	19.35	2.66			
F22-2	78.75	21.23					
F23-1	79.25	4.28	4.60	0.46			
F23-2	79.25	4.93					
F24-1	80.25	10.22	9.67	0.77	12.39	3.84	0.51
F24-2	80.25	9.13					
F25-1	80.25	14.64	15.11	0.67			
F25-2	80.25	15.58					
F27-1	80.75	8.26					
F28-1	81.25	9.20	8.77	0.61	8.13	0.90	0.34
F28-2	81.25	8.33					
F29-1	81.25	7.75	7.50	0.36			
F29-2	81.25	7.25					
F30-1	81.75	9.42	8.62	1.13			
F30-2	81.75	7.83					
F31-1	82.75	17.39	13.66	5.28	12.57	1.54	4.75
F31-2	82.75	9.93					
F33-1	82.75	17.25	11.49	8.15			
F33-2	82.75	5.72					
F35-1	83.25	10.00	0.05	0.37	11.97	2.74	2.08
F35-2	83.25	10.07					
F36-1	83.25	9.78	13.91	5.84			
F36-2	83.25	18.04					
F38-2	83.75	13.19	12.25	1.33	11.90	0.49	0.78
F38-3	83.75	11.30					
F39-1	83.75	12.17	11.56	0.87			
F39-2	83.75	10.94					
F40-2	84.25	10.07			12.95	2.90	1.78
F41-1	84.25	15.00					
F43-1	84.25	10.22	10.91	0.97			
F43-2	84.25	11.59					
F44-1	84.75	11.38	12.79	2.00	12.56	3.36	1.46
F44-2	84.75	14.20					
F45-1	84.75	12.97	15.80	4.00			
F45-2	84.75	18.62					
F46-1	84.75	7.97	9.09	1.59			
F46-2	84.75	10.22					
F48-1	85.25	7.25	7.61	0.51	9.71	2.97	0.65
F48-2	85.25	7.97					
F49-1	85.25	10.87	11.81	1.33			
F49-2	85.25	12.75					
F51-1	85.75	13.77	12.93	1.18			
F51-2	85.75	12.10					
F52-1	86.25	13.33	9.53	5.38	10.43	1.28	1.92
F52-2	86.25	5.72					
F53-1	86.25	11.38	11.34	0.05			
F53-2	86.25	11.30					
F54-2	86.75	12.75	15.29	3.59	18.99	5.23	
F54-3	86.75	17.83					
F55-1	86.75	22.68					
F56-1	88.75	18.55	18.66	0.15			
F56-2	88.75	18.77					
F57-1	89.25	15.65	18.26	3.69			
F57-2	89.25	20.87					
F58-1	89.75	11.38			11.34	0.05	
F59-1	89.75	12.54	11.30	1.74			
F59-2	89.75	10.07					
F60-1	90.75	11.81	13.26	2.05	12.81	0.64	1.43
F60-2	90.75	14.71					
F61-1	90.75	13.77	12.36	2.00			
F61-2	90.75	10.94					
F62-2	91.25	18.19					
F63-1	91.25	13.91	18.15	6.00			
F63-2	91.25	22.39					
F64-1	91.75	23.84	24.02	0.26	16.45	10.71	0.11
F64-2	91.75	24.20					
F65-1	91.75	8.84	8.88	0.05			
F65-2	91.75	8.91					
F67-2	92.25	18.26	17.83	0.61	16.27	2.20	
F67-3	92.25	17.39					
F68-2	92.25	14.71					
F69-1	92.75	8.62	10.33	2.41			
F69-2	92.75	12.03					
F70-1	92.75	14.64	13.30	1.90	12.10	1.57	1.09
F70-2	92.75	11.96					
F71-1	92.75	12.46	12.68	0.31			
F71-2	92.75	12.90					
G2-2	93.25	12.68					
G5-1	94.25	24.86	22.90	2.77			
G5-2	94.25	20.94					
G7-1	95.25	8.04	8.26	0.31			
G7-2	95.25	8.48					
G8-1	96.25	8.84	10.33	2.10			
G8-2	96.25	11.81					
G9-1	97.75	9.64	10.04	0.56			
G9-2	97.75	10.43					
G10-1	98.75	7.90	8.01	0.15			
G10-2	98.75	8.12					
G11-1	99.25	9.93	9.82	0.15			
G11-2	99.25	9.71					
G12-1	100.75	16.01	13.19	4.00			
G12-2	100.75	10.36					
G13-1	101.25	10.80	9.28	2.15			
G13-2	101.25	7.75					
G14-1	102.75	8.41					
G14-2	102.75	7.97					
G15-1	103.25	18.77	16.96	2.56			
G15-2	103.25	15.14					
G17-1	104.25	6.88	7.10	0.31			
G17-2	104.25	7.32					
G18-1	104.75	6.30	8.55	3.18			
G18-2	104.75	10.80					
G19-1	105.25	6.09	6.27	0.26			
G19-2	105.25	6.45					
G19R-1	105.25	8.26	9.46	1.69			
G19R-2	105.25	10.65					
G20-1	105.75	8.12	8.80	0.97			

Table A1. (continued)

Ablation Code	Depth (cm)	Ba/Ca (μmol/mol)	AVE Test	SD Test	AVE Depth	SD Depth	SE Depth
G20-2	105.75	9.49					
G22-1	106.25	9.93	9.78	0.20			
G22-2	106.25	9.64					
G25-1	106.75	8.04	8.59	0.77			
G25-2	106.75	9.13					
G26-1	107.25	6.38	6.99	0.87			
G26-2	107.25	7.61					
G27-1	108.25	1.23	1.38	0.20			
G27-2	108.25	1.52					
G30-1	108.75	5.80	6.81	1.43			
G30-2	108.75	7.83					
G31-1	109.75	7.68	8.30	0.87			
G31-2	109.75	8.91					
G32-1	110.25	6.59	6.38	0.31			
G32-2	110.25	6.16					
G34-1	110.75	6.16	5.76	0.56			
G34-2	110.75	5.36					
G36-1	111.25	8.41	8.62	0.31			
G36-2	111.25	8.84					
G41-1	113.25	13.19	11.30	2.66			
G41-2	113.25	9.42					
G42-2	114.25	4.86					
G43-1	116.25	4.64	4.49	0.20			
G43-2	116.25	4.35					
G46-1	118.25	9.28	9.75	0.67			
G46-2	118.25	10.22					
G47-1	122.25	4.71	4.53	0.26			
G47-2	122.25	4.35					
G51-3	134.25	3.77					
G52-1	136.25	6.59	5.98	0.87			
G52-2	136.25	5.36					
G53-1	140.25	3.19	3.80	0.87			
G53-2	140.25	4.42					
G54-1	142.25	10.00	10.25	0.36			
G54-2	142.25	10.51					

[a]AVE, average; SD, standard deviation; SE, standard error.

7700 years B.P. resulted in an interruption of the sapropel, while the final cooling event at 6100 years B.P. shut sapropel formation down completely with renewed ventilation of the Aegean bottom waters. We propose that the nonlinear response to successive cooling events reflects the existence of two alternate states or stable modes, which alternate according to a hysteresis loop (Figure 8) [*May*, 1977; *Scheffer et al.*, 2001]. We constrain the shape of this hysteresis loop for sapropel initiation and termination by plotting $(Ba/Al)_{sed}$ to characterize the "mode" (sapropel or nonsapropel) and $(Mg/Ca)_{H.\ elegans}$ to characterize a key system variable (temperature). The hysteresis is defined by the forward and backward switch from sapropel to nonsapropel mode occurring at different critical conditions (Figure 8). The sapropel mode is marked by increased water column stratification and enhanced export fluxes. Around 7700 years B.P., the sapropel "interruption" coincides with a cooling event similar to that seen at around 6100 years B.P. Yet, after the temperature perturbation is removed, sapropel formation continues after the 7700 years B.P. event, and not after the 6100 years B.P. event (NB, for clarity, we emphasize again that all ages are reported in radiocarbon convention years, without corrections). Marine and terrestrial $\delta^{18}O$ records exhibit a mean

Table A2. Results of Mn Single Laser Ablation Analyses, With Averages per Test Where Applicable, Standard Deviation, and Standard Error per Depth, Where Applicable[a]

Ablation Code	Depth (cm)	Mn/Ca (μmol/mol)	AVE Test	SD Test	AVE Depth	SD Depth	SE Depth
F2-1	56.25	2.36	2.09	0.39	2.98	1.26	0.30
F2-2	56.25	1.82					
F3-1	56.25	3.82	3.88	0.46			
F3-2	56.25	3.45					
F3-3	56.25	4.36					
F4-1	60.25	2.00	2.18	0.26			
F4-2	60.25	2.36					
F5-2	62.25	2.00	2.73	1.03	2.27	0.64	0.82
F5-3	62.25	3.45					
F6-1	62.25	2.73	1.82	1.29			
F6-2	62.25	0.91					
F8-1	64.25	2.00	1.73	0.39			
F8-3	64.25	1.45					
F9-1	68.25	0.73	1.36	0.90			
F9-2	68.25	2.91					
F9-3	68.25	2.00					
F11-3	70.25	3.64	3.64				
F11-4	70.25	3.64					
F13-2	73.75	4.91					
F15-1	74.25	6.73					
F17-1	75.75	1.27	2.09	1.16			
F17-2	75.75	2.91					
F18-1	76.25	6.18					
F19-1	78.25	3.27	3.82	0.77			
F19-2	78.25	4.36					
F21-1	78.75	2.36	2.09	0.39	4.14	2.89	0.23
F21-2	78.75	1.82					
F22-1	78.75	6.36	6.18	0.26			
F22-2	78.75	6.00					
F23-1	79.25	1.27	1.18	0.13			
F23-2	79.25	1.09					
F24-1	80.25	2.18	2.45	0.39	3.09	0.90	0.18
F24-2	80.25	2.73					
F25-1	80.25	3.64	3.73	0.13			
F25-2	80.25	3.82					
F27-1	80.75	3.82					
F28-1	81.25	6.00	6.27	0.39	3.77	3.54	0.23
F28-2	81.25	6.55					
F29-1	81.25	1.45	1.27	0.26			
F29-2	81.25	1.09					
F30-1	81.75	3.45	3.91	0.64			
F30-2	81.75	4.36					
F31-1	82.75	11.09	7.27	5.40	4.36	4.11	2.00
F31-2	82.75	3.45					
F33-1	82.75	1.27	1.45	0.26			
F33-2	82.75	1.64					
F35-1	83.25	4.36	2.19	67.25	5.77	0.19	1.86
F35-2	83.25	7.45					
F36-1	83.25	3.45	5.64	3.09			
F36-2	83.25	7.82					
F38-2	83.75	1.09	1.91	1.16	2.05	0.19	0.59
F38-3	83.75	2.73					
F39-1	83.75	1.82	2.18	0.51			
F39-2	83.75	2.55					
F40-2	84.25	4.36			4.50	0.19	1.00
F41-1	84.25	4.36					
F43-1	84.25	3.64	4.64	1.41			
F43-2	84.25	5.64					
F44-1	84.75	3.64	4.82	1.67	3.76	0.92	0.69
F44-2	84.75	6.00					
F45-1	84.75	2.18	3.27	1.54			
F45-2	84.75	4.36					
F46-1	84.75	3.45	3.18	0.39			
F46-2	84.75	2.91					
F48-1	85.25	3.27	3.09	0.26	2.59	0.71	0.41
F48-2	85.25	2.91					

Table A2. (continued)

Ablation Code	Depth (cm)	Mn/Ca (μmol/mol)	AVE Test	SD Test	AVE Depth	SD Depth	SE Depth
F49-1	85.25	2.73	2.09	0.90			
F49-2	85.25	1.45					
F51-1	85.75	6.91	5.45	2.06			
F51-2	85.75	4.00	0.00	0.00			
F52-1	86.25	4.55	3.73	1.16	3.00	1.03	0.45
F52-2	86.25	2.91					
F53-1	86.25	2.18	2.27	0.13			
F53-2	86.25	2.36					
F54-2	86.75	5.82	6.64	1.16	5.59	1.48	
F54-3	86.75	7.45					
F55-1	86.75	4.55					
F56-1	88.75	5.64	7.09	2.06			
F56-2	88.75	8.55					
F57-1	89.25	3.45	5.27	2.57			
F57-2	89.25	7.09					
F58-1	89.75	4.91			4.32	0.84	
F59-1	89.75	6.00	3.73	3.21			
F59-2	89.75	1.45					
F60-1	90.75	6.00	4.91	1.54	4.23	0.96	0.95
F60-2	90.75	3.82					
F61-1	90.75	4.36	3.55	1.16			
F61-2	90.75	2.73					
F62-2	91.25	3.82					
F63-1	91.25	2.36	4.73	3.34			
F63-2	91.25	7.09					
F64-1	91.75	6.36	6.27	0.13	4.00	3.21	0.18
F64-2	91.75	6.18					
F65-1	91.75	2.00	1.73	0.39			
F65-2	91.75	1.45					
F67-2	92.25	8.55	7.73	1.16	5.95	2.51	
F67-3	92.25	6.91					
F68-2	92.25	4.18					
F69-1	92.75	3.09	3.55	0.64			
F69-2	92.75	4.00					
F70-1	92.75	5.45	6.09	0.90	5.27	1.50	0.67
F70-2	92.75	6.73					
F71-1	92.75	7.09	6.18	1.29			
F71-2	92.75	5.27					
G2-2	93.25	5.09					
G5-1	94.25	8.00	8.18	0.26			
G5-2	94.25	8.36					
G7-1	95.25	2.91	4.00	1.54			
G7-2	95.25	5.09					
G8-1	96.25	1.82	3.45	2.31			
G8-2	96.25	5.09					
G9-1	97.75	3.09	3.27	0.26			
G9-2	97.75	3.45					
G10-1	98.75	4.73	4.09	0.90			
G10-2	98.75	3.45					
G11-1	99.25	1.64	1.27	0.51			
G11-2	99.25	0.91					
G12-1	100.75	6.91	6.18	1.03			
G12-2	100.75	5.45					
G13-1	101.25	2.18	2.18	0.00			
G13-2	101.25	2.18					
G14-1	102.75	2.18					
G14-2	102.75	1.27					
G15-1	103.25	4.91	3.55	1.93			
G15-2	103.25	2.18					
G17-1	104.25	1.27	1.18	0.13			
G17-2	104.25	1.09					
G18-1	104.75	1.27	2.55	1.80			
G18-2	104.75	3.82					
G19-1	105.25	3.82	3.18	0.90			
G19-2	105.25	2.55					
G19R-1	105.25	2.91	2.91	0.00			
G19R-2	105.25	2.91					
G20-1	105.75	0.91	1.55	0.90			
G20-2	105.75	2.18					
G22-1	106.25	1.27	1.36	0.13			
G22-2	106.25	1.45					
G25-1	106.75	1.64	1.64	0.00			
G25-2	106.75	1.64					
G26-1	107.25	2.36	2.45	0.13			
G26-2	107.25	2.55					
G27-1	108.25	2.91	2.27	0.90			
G27-2	108.25	1.64					
G30-1	108.75	2.36	3.27	1.29			
G30-2	108.75	4.18					
G31-1	109.75	2.91	2.82	0.13			
G31-2	109.75	2.73					
G32-1	110.25	2.18	1.91	0.39			
G32-2	110.25	1.64					
G34-1	110.75	1.45	2.00	0.77			
G34-2	110.75	2.55					
G36-1	111.25	3.82	4.73	1.29			
G36-2	111.25	5.64					
G41-1	113.25	2.55	2.45	0.13			
G41-2	113.25	2.36					
G42-2	114.25	2.55					
G43-1	116.25	0.55	0.55	0.00			
G43-2	116.25	0.55					
G46-1	118.25	2.55	3.27	1.03			
G46-2	118.25	4.00					
G47-1	122.25	3.82	2.64	1.67			
G47-2	122.25	1.45					
G51-3	134.25	8.00					
G52-1	136.25	1.64	2.00	0.51			
G52-2	136.25	2.36					
G53-1	140.25	2.00	2.09	0.13			
G53-2	140.25	2.18					
G54-1	142.25	8.00	7.18	1.16			
G54-2	142.25	6.36					

[a]AVE, average; SD, standard deviation; SE, standard error.

δ^{18}O depletion after ~7 kyr B.P., suggesting a weakening monsoon [*Rohling*, 1999; *Bar-Matthews et al.*, 2000; *Rohling et al.*, 2002; *Arz et al.*, 2003; *De Lange et al.*, 2008] which, in interplay with the 6100 years B.P. event, could have facilitated a permanent stop to sapropel formation.

[38] Based on the $(Ba/Al)_{sed}$ versus $(Mg/Ca)_{H.\ elegans}$ plot (Figure 8), the critical thresholds defining the sapropel and nonsapropel mode, can be estimated. The $(Mg/Ca)_{H.\ elegans}$ values reflect bottom water conditions, hence winter temperatures. Although temperature was clearly not the only factor involved, the critical value required to go into sapropel mode was about 14°C, whereas the temperature tipping the system back to its nonsapropel mode was on the order of 10°C. While this temperature range is relatively limited, it was enough to maintain the stratified conditions first initiated by freshwater input, and thus keep the Aegean in its sapropel state for several thousand years.

5. Conclusions and Implications

[39] This study introduces a promising new application of LA-ICP-MS to benthic foraminifera. The integrated study of dissolved and particulate trace elements allows the better

Table A3. Results of Mg Single Laser Ablation Analyses, With Averages per Test Where Applicable, Standard Deviation and Standard Error per Depth, Where Applicable[a]

Ablation Code	Depth (cm)	Mg/Ca (mmol/mol)	AVE Test	SD Test	AVE Depth	SD Depth	SE Depth
F2-1	56.25	3.51	3.12	0.55	2.92	0.28	0.21
F2-2	56.25	2.73					
F3-1	56.25	2.75	2.72	0.04	0.00	0.00	0.00
F3-2	56.25	2.68					
F3-3	56.25	2.72					
F4-1	60.25	3.09	3.04	0.08			
F4-2	60.25	2.98					
F5-2	62.25	1.59	1.70	0.15	1.87	0.24	0.14
F5-3	62.25	1.81					
F6-1	62.25	1.87	2.04	0.24			
F6-2	62.25	2.21					
F8-1	64.25	2.27	2.20	0.09			
F8-3	64.25	2.13					
F9-1	68.25	2.09	2.08				
F9-2	68.25	2.91					
F9-3	68.25	2.08					
F11-3	70.25	2.92	2.90	0.04			
F11-4	70.25	2.87					
F13-2	73.75	3.06					
F15-1	74.25	3.62					
F17-1	75.75	3.21	3.19	0.03			
F17-2	75.75	3.17					
F18-1	76.25	3.38					
F19-1	78.25	3.17	3.45	0.39			
F19-2	78.25	3.72					
F21-1	78.75	3.17	3.04	0.18	3.87	1.18	0.21
F21-2	78.75	2.91					
F22-1	78.75	4.41	4.71	0.42			
F22-2	78.75	5.00					
F23-1	79.25	2.44	2.72	0.39			
F23-2	79.25	2.99					
F24-1	80.25	2.38	2.58	0.28	2.67	0.14	0.11
F24-2	80.25	2.77					
F25-1	80.25	2.74	2.77	0.04			
F25-2	80.25	2.80					
F27-1	80.75	1.95					
F28-1	81.25	2.93	2.81	0.16	2.52	0.41	0.15
F28-2	81.25	2.69					
F29-1	81.25	2.42	2.22	0.27			
F29-2	81.25	2.03					
F30-1	81.75	3.24	3.11	0.20			
F30-2	81.75	2.97					
F31-1	82.75	3.29	2.94	0.50	2.64	0.43	0.39
F31-2	82.75	2.59					
F33-1	82.75	2.76	2.33	0.60			
F33-2	82.75	1.91					
F35-1	83.25	2.54	2.73	0.27	2.82	0.13	0.46
F35-2	83.25	2.92					
F36-1	83.25	2.20	2.92	1.02			
F36-2	83.25	3.64					
F38-2	83.75	2.28	2.64	0.52	2.72	0.10	0.20
F38-3	83.75	3.01					
F39-1	83.75	2.83	2.79	0.06			
F39-2	83.75	2.75					
F40-2	84.25	2.50			3.34	0.07	0.53
F41-1	84.25	3.29					
F43-1	84.25	3.18	3.38	0.29			
F43-2	84.25	3.59					
F44-1	84.75	2.83	2.83		2.83		0.17
F44-2	84.75	2.83					
F45-1	84.75	2.71	2.82	0.17			
F45-2	84.75	2.94					
F46-1	84.75	2.31	2.83	0.74			
F46-2	84.75	3.35					
F48-1	85.25	2.75	2.47	0.40	2.89	0.60	0.27
F48-2	85.25	2.18					
F49-1	85.25	3.58	3.32	0.37			
F49-2	85.25	3.06					
F51-1	85.75	3.64	3.21	0.61			
F51-2	85.75	2.78					
F52-1	86.25	3.44	2.91	0.75	2.84	0.11	0.28
F52-2	86.25	2.38					
F53-1	86.25	2.79	2.76	0.04			
F53-2	86.25	2.74					
F54-2	86.75	3.24	3.72	0.68			
F54-3	86.75	4.20					
F55-1	86.75	3.65			3.69	0.05	
F56-1	88.75	3.13	3.22	0.12			
F56-2	88.75	3.30					
F57-1	89.25	3.20	3.43	0.32			
F57-2	89.25	3.66					
F58-1	89.75	2.81	2.32	0.41	2.57	0.34	0.36
F59-1	89.75	2.61					
F59-2	89.75	2.04					
F60-1	90.75	3.24	3.01	0.32	2.75	0.37	0.35
F60-2	90.75	2.79					
F61-1	90.75	2.96	2.49	0.67			
F61-2	90.75	2.01					
F62-2	91.25	3.11	3.30	0.32	3.21	0.17	
F63-1	91.25	3.07					
F63-2	91.25	3.53					
F64-1	91.75	3.63	3.55	0.11	3.41	0.20	0.07
F64-2	91.75	3.47					
F65-1	91.75	3.33	3.27	0.09			
F65-2	91.75	3.21					
F67-2	92.25	4.97	5.14	0.24	4.64	0.70	0.35
F67-3	92.25	5.31					
F68-2	92.25	4.15					
F69-1	92.75	2.19	2.86	0.95	3.03	0.53	0.27
F69-2	92.75	3.53					
F70-1	92.75	3.70	3.62	0.11			
F70-2	92.75	3.54					
F71-1	92.75	2.82	2.60	0.31			
F71-2	92.75	2.37					
G2-2	93.25	3.14					
G5-1	94.25	3.73	3.46	0.38			
G5-2	94.25	3.19					
G7-1	95.25	2.83	2.76	0.10			
G7-2	95.25	2.69					
G8-1	96.25	2.81	2.91	0.15			
G8-2	96.25	3.02					
G9-1	97.75	3.15	3.23	0.11			
G9-2	97.75	3.31					
G10-1	98.75	2.37	2.53	0.23			
G10-2	98.75	2.69					
G11-1	99.25	3.64	3.47	0.24			
G11-2	99.25	3.30					
G12-1	100.75	3.49	3.09	0.56			
G12-2	100.75	2.69					
G13-1	101.25	3.78	3.00	1.11			
G13-2	101.25	2.21					
G14-1	102.75	2.98	2.98	0.24			
G14-2	102.75	2.64					
G15-1	103.25	2.88	2.70	0.25			
G15-2	103.25	2.52					
G17-1	104.25	3.54	3.38	0.23			
G17-2	104.25	3.21					
G18-1	104.75	2.38	3.01	0.90			
G18-2	104.75	3.65					
G19-1	105.25	2.95	2.76	0.26			
G19-2	105.25	2.58					
G19R-1	105.25	2.78	2.81	0.04			
G19R-2	105.25	2.84					
G20-1	105.75	2.41	2.70	0.40			

Table A3. (continued)

Ablation Code	Depth (cm)	Mg/Ca (mmol/mol)	AVE Test	SD Test	AVE Depth	SD Depth	SE Depth
G20-2	105.75	2.98					
G22-1	106.25	2.55	2.57	0.03			
G22-2	106.25	2.59					
G25-1	106.75	2.52	3.01	0.70			
G25-2	106.75	3.50					
G26-1	107.25	2.03	2.14	0.15			
G26-2	107.25	2.24					
G27-1	108.25	1.33	1.40	0.11			
G27-2	108.25	1.48					
G30-1	108.75	3.85	3.73	0.17			
G30-2	108.75	3.62					
G31-1	109.75	1.88	2.16	0.39			
G31-2	109.75	2.44					
G32-1	110.25	3.03	2.71	0.45			
G32-2	110.25	2.40					
G34-1	110.75	2.42	2.54	0.18			
G34-2	110.75	2.67					
G36-1	111.25	2.82	2.53	0.41			
G36-2	111.25	2.23					
G41-1	113.25	2.66	2.81	0.21			
G41-2	113.25	2.96					
G42-2	114.25	2.81					
G43-1	116.25	3.07	2.73	0.48			
G43-2	116.25	2.39					
G46-1	118.25	2.90	2.97	0.09			
G46-2	118.25	3.03					
G47-1	122.25	2.16	1.96	0.28			
G47-2	122.25	1.76					
G51-3	134.25	3.07					
G52-1	136.25	2.60	2.72	0.17			
G52-2	136.25	2.84					
G53-1	140.25	1.15	1.50	0.49			
G53-2	140.25	1.84					
G54-1	142.25	3.24	3.28	0.07			
G54-2	142.25	3.33					

[a]AVE, average; SD, standard deviation; SE, standard error.

constraint of physiochemical processes at play at the sediment water interface. Trace metal records from *H. elegans* tests show past variations in bottom water chemistry and temperature before, during and after sapropel S1 deposition. Enhanced export fluxes as indicated by our sedimentary $(Ba/Al)_{sed}$ and foraminiferal $(Ba/Ca)_{H.\ elegans}$ occurred particularly during the first phase of sapropel formation. The reduced $(Mn/Al)_{sed}$ and concomitantly enhanced foraminiferal $(Mn/Ca)_{H.\ elegans}$ clearly point to reduced bottom water oxygenation during sapropel deposition. Three distinct cooling events are recorded by the (Mg/Ca) record of *H. elegans*. The last two of these events lead to sapropel interruption and termination, respectively. We propose a hysteresis loop with two stable modes, the sapropel mode and the nonsapropel mode. The stability of the sapropel mode is controlled by "slow variables" such as export productivity and stratification, but is also sensitive to episodic perturbations, such as abrupt cooling events.

Appendix A

[40] We present the results of single laser ablation analyses, including averages per test, standard deviation, and standard error per depth, for Ba (Table A1), Mn (Table A2), and Mg (Table A3).

[41] **Acknowledgments.** We thank two anonymous reviewers for their suggestions, which greatly improved this manuscript. Also, the support of the crew and captain of R/V *Aegeo* during the sampling campaign for core SLA-9 is gratefully acknowledged. Paul Mason and Gijs Nobbe are thanked for their assistance with LA-ICP-MS. This is publication DW-2009-5004 of the Darwin Center for Biogeosciences, which partially funded this project.

References

Abu-Zied, R. H., E. L. Rohling, F. J. Jorissen, C. Fontanier, J. S. L. Casford, and S. Cooke (2008), Benthic foraminiferal response to changes in bottom-water oxygenation and organic carbon flux in the eastern Mediterranean during LGM to recent times, *Mar. Micropaleontol.*, *67*, 46–68, doi:10.1016/j.marmicro.2007.08.006.

Aksu, A. E., T. Abrajano, P. J. Mudie, and D. Yasar (1999), Organic geochemical and palynological evidence for terrigenous origin of the organic matter in Aegean Sea sapropel S1, *Mar. Geol.*, *153*, 303–318, doi:10.1016/S0025-3227(98)00077-2.

Antoine, D., A. Morel, and J.-M. André (1995), Algal pigment distribution and primary production in the eastern Mediterranean as derived from coastal zone color scanner observations, *J. Geophys. Res.*, *100*, 16,193–16,209, doi:10.1029/95JC00466.

Arz, H. W., F. Lamy, J. Pätzold, P. J. Müller, and M. Prins (2003), Mediterranean moisture source for an early Holocene humid period in the northern Red Sea, *Science*, *300*, 118–121, doi:10.1126/science.1080325.

Barker, S., M. Greaves, and H. Elderfield (2003), A study of cleaning procedures used for foraminiferal Mg/Ca paleothermometry, *Geochem. Geophys. Geosyst.*, *4*(9), 8407, doi:10.1029/2003GC000559.

Bar-Matthews, M., A. Ayalon, and A. Kaufman (2000), Timing and hydrological conditions of Sapropel events in the eastern Mediterranean, as evident from speleothems, Soreq cave, Israel, *Chem. Geol.*, *169*, 145–156, doi:10.1016/S0009-2541(99)00232-6.

Bishop, J. K. B. (1988), The barite-opal-organic carbon association in oceanic particulate matter, *Nature*, *332*, 341–343, doi:10.1038/332341a0.

Boyle, E. A. (1983), Manganese carbonate overgrowths on foraminifera tests, *Geochim. Cosmochim. Acta*, *47*, 1815–1819, doi:10.1016/0016-7037(83)90029-7.

Boyle, E. A., L. Labeyrie, and J.-C. Duplessy (1995), Calcitic foraminiferal data confirmed by cadmium in aragonitic *Hoeglundina*: Application to the Last Glacial Maximum in the northern Indian Ocean, *Paleoceanography*, *10*, 881–900, doi:10.1029/95PA01625.

Burdige, D. J. (2005), Burial of terrestrial organic matter in marine sediments: A re-assessment, *Global Biogeochem. Cycles*, *19*, GB4011, doi:10.1029/2004GB002368.

Burdige, D. J. (2006), Geochemistry of Marine Sediments, Princeton Univ. Press, Princeton, N. J.

Cacho, I., J. O. Grimalt, M. Canals, L. Sbaffi, N. J. Shackleton, J. Schönfeld, and R. Zahn (2001), Variability of the western Mediterranean Sea surface temperatures during the last 25,000 years and its connection with the Northern Hemisphere climatic changes, *Paleoceanography*, *16*(1), 40–52, doi:10.1029/2000PA000502.

Casford, J. S. L., E. J. Rohling, R. H. Abu-Zied, S. Cooke, C. Fontanier, M. J. Leng, and V. Lykousis (2002), Circulation changes and nutrient concentrations in the late Quaternary Aegean Sea: A nonsteady state concept for sapropel formation, *Paleoceanography*, *17*(2), 1024, doi:10.1029/2000PA000601.

Casford, J. S. L., E. J. Rohling, R. H. Abu-Zied, C. Fontanier, F. J. Jorissen, M. J. Leng, G. Schmiedl, and J. Thomson (2003), A dynamic concept for eastern Mediterranean

circulation and oxygenation during sapropel formation, *Palaeogeogr. Palaeoclimatol. Palaeoecol.*, *190*, 103–119, doi:10.1016/S0031-0182(02)00601-6.

Casford, J. S. L., R. H. Abu-Zied, E. J. Rohling, S. Cooke, C. Fontanier, M. J. Leng, A. Millard, and J. Thomson (2007), A stratigraphically controlled multi-proxy chronostratigraphy for the eastern Mediterranean, *Paleoceanography*, *22*, PA4215, doi:10.1029/2007PA001422.

Church, T. M., and K. Wolgemuth (1972), Marine barite saturation, *Earth Planet. Sci. Lett.*, *15*, 35–44, doi:10.1016/0012-821X(72)90026-X.

Cita, M. B., C. Vergnaud-Grazzini, C. Robert, H. Chamley, N. Ciaranfi, and S. d'Onofrio (1977), Paleoclimatic record of a long deep sea core from the eastern Mediterranean, *Quat. Res.*, *8*, 205–235, doi:10.1016/0033-5894(77)90046-1.

Dehairs, F., R. Chesselet, and J. Jedwab (1980), Discrete suspended particles of barite and the barium cycle in the open ocean, *Earth Planet. Sci. Lett.*, *49*(2), 528–550, doi:10.1016/0012-821X(80)90094-1.

De Lange, G. J., G. Catalano, G. P. Klinkhammer, and G. W. Luther III (1990), The interface between oxic seawater and the anoxic Bannock brine; its sharpness and the consequences for the redox-related cycling of Mn and Ba, *Mar. Chem.*, *31*(1–3), 205–217, doi:10.1016/0304-4203(90)90039-F.

De Lange, G. J., J. Thomson, A. Reitz, C. P. Slomp, M. Speranza Principato, E. Erba, and C. Corselli (2008), Synchronous basin-wide formation and redox-controlled preservation of a Mediterranean sapropel, *Nat. Geosci.*, *1*, 606–610, doi:10.1038/ngeo283.

De Rijk, S., A. Hayes, and E. J. Rohling (1999), Eastern Mediterranean sapropel S1 interruption: An expression of the onset of climatic deterioration around 7 ka BP, *Mar. Geol.*, *153*, 337–343, doi:10.1016/S0025-3227(98)00075-9.

De Rijk, S., F. J. Jorissen, E. J. Rohling, and S. R. Troelstra (2000), Organic flux control on bathymetric zonation of Mediterranean benthic foraminifera, *Mar. Micropaleontol.*, *40*, 151–166, doi:10.1016/S0377-8398(00)00037-2.

Douglas, R. G., and H. L. Heitman (1979), Slope and basin benthic foraminifera of the California Borderland, *Spec. Publ. Soc. Econ. Paleontol. Mineral.*, *27*, 231–246.

Dymond, J., and R. Collier (1996), Particulate barium fluxes and their relationships to biological productivity, *Deep Sea Res.*, Pari II, *43*, 1283–1308, doi:10.1016/0967-0645(96)00011-2.

Epstein, S., R. Buchsbaum, H. A. Lowenstam, and H. C. Urey (1951), Carbonate-water isotopic temperature scale, *Geol. Soc. Am. Bull.*, *62*, 417–426, doi:10.1130/0016-7606(1951)62[417:CITS]2.0.CO;2.

Fontanier, C., F. J. Jorissen, L. Licari, A. Alexandre, P. Anschutz, and P. Carbonel (2002), Live benthic foraminiferal faunas from the Bay of Biscay: Faunal density, composition, and microhabitats, *Deep Sea Res.*, Part I, *49*, 751–785, doi:10.1016/S0967-0637(01)00078-4.

Froelich, P. N., G. P. Klinkhammer, M. L. Bender, N. A. Luedtke, G. R. Heath, D. Cullen, P. Dauphin, D. Hammond, B. Hartman, and V. Maynard (1979), Early oxidation of organic pelagic sediments of the eastern equatorial Atlantic: Suboxic diagenesis, *Geochim. Cosmochim. Acta*, *43*(7), 1075–1090, doi:10.1016/0016-7037(79)90095-4.

Geraga, M., S. Tsaila-Monopolis, C. Ioakim, G. Papatheodorou, and G. Ferentinos (2000), Evaluation of palaeoenvironmental changes during the last 18,000 years in the Myrtoon basin, SW Aegean Sea, *Palaeogeogr. Palaeoclimatol. Palaeoecol.*, *156*, 1–17, doi:10.1016/S0031-0182(99)00123-6.

Hall, J. M., and L.-H. Chan (2004), Ba/Ca in *Neogloboquadrina pachyderma* as an indicator of deglacial meltwater discharge into the western Arctic Ocean, *Paleoceanography*, *19*, PA1017, doi:10.1029/2003PA000910.

Hathorne, E. C., R. H. James, P. Savage, and O. Alard (2008), Physical and chemical characteristics of particles produced by laser ablation of biogenic calcium carbonate, *J. Anal. At. Spectrom.*, *23*, 240–243, doi:10.1039/b706727e.

Hilgen, F. J. (1991), Astronomical calibration of Gauss to Matuyama sapropels in the Mediterranean and implication for the geomagnetic polarity time scale, *Earth Planet. Sci. Lett.*, *104*, 226–244, doi:10.1016/0012-821X(91)90206-W.

Hughes, J. A., A. J. Gooday, and J. W. Murray (2000), Distribution of live benthic foraminifera at three oceanographically dissimilar sites in the northeast Atlantic: Preliminary results, *Hydrobiologica*, *440*(1–3), *227–238*, doi:10.1023/A:1004131413665.

Jorissen, F. J. (1999), Benthic foraminiferal successions across Late Quaternary Mediterranean sapropels, *Mar. Geol.*, *153*, 91–101, doi:10.1016/S0025-3227(98)00088-7.

Jorissen, F. J., I. Wittling, J. P. Peypouquet, C. Rabouille, and J. C. Relaxans (1998), Live benthic foraminiferal faunas off Cape Blanc, NW-Africa: Community structure and microhabitats, *Deep Sea Res.*, Part I, *45*(12), 2157–2188, doi:10.1016/S0967-0637(98)00056-9.

Jorissen, F., C. Fontanier, and E. Thomas (2007), Paleoceanographical proxies based on deep-sea benthic foraminiferal assemblage characteristics, in *Proxies in Late Cenozoic Paleoceanography*, *Dev. Mar. Geol.*, vol. 1, edited by C. Hillaire-Marcel and A. de Vernal, pp. 263–325, Elsevier, New York, doi:10.1016/S1572-5480(07)01012-3.

Kidd, R. B., M. B. Cita, and W. B. F. Ryan (1978), Stratigraphy of eastern Mediterranean sapropel sequences recovered during DSDP Leg 42A and their palaeoenvironmental significance, *Initial Rep. Deep Sea Drill. Proj.*, *42A*, 421–443.

Koho, K. A., R. Garcia, H. C. de Stigter, E. Epping, E. Koning, T. J. Kouwenhoven, and G. J. van der Zwaan (2008), Sedimentary labile organic carbon and pore water redox control on species distribution of benthic foraminifera: A case study from Lisbon–Setúbal Canyon (southern Portugal), *Prog. Oceanogr.*, *79*(1), 55–82, doi:10.1016/j.pocean.2008.07.004.

Kuhnt, T., G. Schmiedl, W. Ehrmann, Y. Hamann, and C. Hemleben (2007), Deep-sea ecosystem variability of the Aegean Sea during the past 22 kyr as revealed by benthic foraminifera, *Mar. Micropaleontol.*, *64*, 141–162, doi:10.1016/j.marmicro.2007.04.003.

Lascaratos, A., W. Roether, K. Nittis, and B. Klein (1999), Recent changes in deep water formation and spreading in the eastern Mediterranean Sea: A review, *Prog. Oceanogr.*, *44*(1–3), 5–36, doi:10.1016/S0079-6611(99)00019-1.

Lea, D., and E. Boyle (1989), Barium content of benthic foraminifera controlled by bottom-water composition, *Nature*, *338*, 751–753, doi:10.1038/338751a0.

Lear, C. H., H. Elderfield, and P. A. Wilson (2000), Cenozoic deep-sea temperatures and global ice volumes from Mg/Ca in benthic foraminiferal calcite, *Science*, *287*, 269–272, doi:10.1126/science.287.5451.269.

Libes, S. M. (2009), *Introduction to Marine Biogeochemistry*, pp. 316–317, Academic, San Diego, Calif.

Lohmann, G. (1995), A model for variation in the chemistry of planktonic foraminifera due to secondary calcification and selective dissolution, *Paleoceanography*, *10*(3), 445–457, doi:10.1029/95PA00059.

Lutze, G. F., and W. T. Coulbourn (1984), Recent foraminifera from the continental margin of northwest Africa: Community structure and distribution, *Mar. Micropaleontol.*, *8*(5), 361–401, doi:10.1016/0377-8398(84)90002-1.

Mackensen, A., and R. G. Douglas (1989), Down-core distribution of live and dead deep-water benthic foraminifera in box cores from the Weddell Sea and the California continental borderland, *Deep Sea Res.*, Part A, *36*, 879–900, doi:10.1016/0198-0149(89)90034-4.

Marino, G., E. J. Rohling, W. I. C. Rijpstra, F. Sangiorgi, S. Schouten, and J. Sinninghe-Damste (2007), Aegean Sea as driver of hydrographic and ecological changes in the eastern Mediterranean, *Geology*, *35*(8), 675–678, doi:10.1130/G23831A.1.

Martin, J. M., and M. Meybeck (1979), Elemental mass-balance of material carried by major world rivers, *Mar. Chem.*, *7*, 173–206, doi:10.1016/0304-4203(79)90039-2.

May, R. M. (1977), Thresholds and breakpoints in ecosystems with a multiplicity of stable states, *Nature*, *269*, 471–477, doi:10.1038/269471a0.

Mercone, D., J. Thomson, R. H. Abu-Zied, I. W. Croudace, and E. J. Rohling (2001), High-resolution geochemical and micropalaeontological profiling of the most recent eastern Mediterranean sapropel, *Mar. Geol.*, *177*, 25–44, doi:10.1016/S0025-3227(01)00122-0.

Millero, F. J., and D. R. Schreiber (1982), Use of the ion pairing model to estimate activity coefficients of the ionic components of natural waters, *Am. J. Sci.*, *282*, 1508–1540, doi:10.2475/ajs.282.9.1508.

Olausson, E. (1961), Studies of deep-sea cores, in *Reports of the Swedish Deep-Sea Expedition 1947–1948*, vol. 8, pp. 353–391, Swed. Nat. Sci. Res. Counc., Stockholm.

Parker, F. L. (1958), Eastern Mediterranean foraminifera, in *Reports of the Swedish Deep-Sea Expedition 1947–1948*, vol. 8, pp. 217–283, Swed. Nat. Sci. Res. Counc., Stockholm.

Passier, H. F., J. J. Middelburg, B. J. H. van Os, and G. J. de Lange (1996), Diagenetic pyritisation under eastern Mediterranean sapropels caused by downward sulphide diffusion, *Geochim. Cosmochim. Acta*, *60*, 751–763, doi:10.1016/0016-7037(95)00419-X.

Pearce, N. J. G., W. T. Perkins, J. A. Westgate, M. P. Gorton, S. E. Jackson, C. R. Neal, and S. P. Chenery (1997), A compilation of new and published major and trace element data for NIST SRM 610 and NIST SRM 612 glass reference materials, *Geostand. Newsl.*, *21*, 115–144, doi:10.1111/j.1751-908X.1997.tb00538.x.

Reichart, G.-J., F. Jorissen, P. R. D. Mason, and P. Anschutz (2003), Single foraminiferal test chemistry records the marine environment,

Geology, *31*, 355–358, doi:10.1130/0091-7613(2003)031<0355:SFTCRT>2.0.CO;2.

Reitz, A., J. Thomson, G. J. de Lange, and C. Hensen (2006), Source and development of large manganese enrichments above eastern Mediterranean sapropel S1, *Paleoceanography*, *21*, PA3007, doi:10.1029/2005PA001169.

Roether, W., B. B. Manca, B. Klein, D. Bregant, D. Georgopoulos, V. Beitzel, V. Kovacevic, and A. Luchetta (1996), Recent changes in eastern Mediterranean deep waters, *Science*, *271*, 333–335, doi:10.1126/science.271.5247.333.

Rohling, E. J. (1994), Review and new aspects concerning the formation of eastern Mediterranean sapropels, *Mar. Geol.*, *122*, 1–28, doi:10.1016/0025-3227(94)90202-X.

Rohling, E. J. (1999), Environmental control on Mediterranean salinity and $\delta^{18}O$, *Paleoceanography*, *14*(6), 706–715, doi:10.1029/1999PA900042.

Rohling, E. J., and W. C. Gieskes (1989), Late Quaternary changes in Mediterranean intermediate water density and formation rate, *Paleoceanography*, *4*, 531–545, doi:10.1029/PA004i005p00531.

Rohling, E. J., and F. J. Hilgen (1991), The eastern Mediterranean climate at times of sapropel formation: A review, *Geol. Mijnbouw*, *70*, 253–264.

Rohling, E. J., F. Jorissen, and H. C. De Stigter (1997), 200 year interruption of Holocene sapropel formation in the Adriatic Sea, *J. Micropalaeontol.*, *16*, 97–108, doi:10.1144/jm.16.2.97.

Rohling, E. J., P. A. Mayewski, R. H. Abu-Zied, J. S. L. Casford, and A. Hayes (2002), Holocene atmosphere-ocean interactions: Records from Greenland and the Aegean Sea, *Clim. Dyn.*, *18*, 587–593, doi:10.1007/s00382-001-0194-8.

Rohling, E. J., et al. (2004), Reconstructing past planktic foraminiferal habitats using stable isotope data: A case history for Mediterranean sapropel S5, *Mar. Micropaleontol.*, *50*, 89–123, doi:10.1016/S0377-8398(03)00068-9.

Rosenthal, Y., E. A. Boyle, and N. Slowey (1997), Temperature control on the incorporation of magnesium, strontium, fluorine, and cadmium into benthic foraminiferal shells from Little Bahama Bank: Prospects for thermocline paleoceanography, *Geochim. Cosmochim. Acta*, *61*, 3633–3643, doi:10.1016/S0016-7037(97)00181-6.

Rosenthal, Y., C. H. Lear, D. W. Oppo, and B. K. Linsley (2006), Temperature and carbonate ion effects on Mg/Ca and Sr/Ca ratios in benthic foraminifera: Aragonitic species *Hoeglundina elegans*, *Paleoceanography*, *21*, PA1007, doi:10.1029/2005PA001158.

Rossignol-Strick, M., W. Nesteroff, P. Olive, and C. Vergnaud-Grazzini (1982), After the deluge: Mediterranean stagnation and sapropel formation, *Nature*, *295*, 105–110, doi:10.1038/295105a0.

Ruddiman, W. F. (1971), Pleistocene sedimentation in the equatorial Atlantic: Stratigraphy and faunal paleoclimatology, *Geol. Soc. Am. Bull.*, *82*, 283–302, doi:10.1130/0016-7606(1971)82[283:PSITEA]2.0.CO;2.

Sachs, J. P., and D. J. Repeta (1999), Oligotrophy and nitrogen fixation during eastern Mediterranean sapropel events, *Science*, *286*, 2485–2488, doi:10.1126/science.286.5449.2485.

Sadekov, A. Y., S. M. Eggins, and P. De Deckker (2005), Characterization of Mg/Ca distributions in planktonic foraminifera species by electron microprobe mapping, *Geochem. Geophys. Geosyst.*, *6*, Q12P06, doi:10.1029/2005GC000973.

Scheffer, M., S. Carpenter, J. A. Foley, C. Folke, and B. Walker (2001), Catastrophic shifts in ecosystems, *Nature*, *413*, 591–596, doi:10.1038/35098000.

Schenau, S. J., M. A. Prins, G. J. De Lange, and C. Monnin (2001), Barium accumulation in the Arabian Sea: Controls on barite preservation in marine sediments, *Geochim. Cosmochim. Acta*, *65*, 1545–1556, doi:10.1016/S0016-7037(01)00547-6.

Schönfeld, J. (2001), Benthic foraminifera and pore-water oxygen profiles: A re-assessment of species boundary conditions at the western Iberian margin, *J. Foraminiferal Res.*, *31*(2), 86–107, doi:10.2113/0310086.

Slomp, C. P., J. Thomson, and G. J. de Lange (2004), Controls on phosphorus regeneration and burial during formation of eastern Mediterranean sapropels, *Mar. Geol.*, *203*, 141–159, doi:10.1016/S0025-3227(03)00335-9.

Theocharis, A. (1989), Deep water formation and circulation in the Aegean sea, in *Reports in Meteorology and Oceanography*, edited by H. Charnock, pp. 335–359, Harvard Univ., Cambridge, Mass.

Thomson, J., N. C. Higgs, T. R. S. Wilson, I. W. Croudace, G. J. de Lange, and P. J. M. van Santvoort (1995), Redistribution and geochemical behaviour of redox-sensitive elements around S1, the most recent eastern Mediterranean sapropel, *Geochim. Cosmochim. Acta*, *59*, 3487–3501, doi:10.1016/0016-7037(95)00232-O.

Thomson, J., D. Mercone, G. J. De Lange, and P. J. M. Van Santvoort (1999), Review of recent advances in the interpretation of eastern Mediterranean sapropel S1 from geochemical evidence, *Mar. Geol.*, *153*, 77–89, doi:10.1016/S0025-3227(98)00089-9.

van Santvoort, P. J. M., G. J. de Lange, J. Thomson, H. Cussen, T. R. S. Wilson, M. Krom, and K. Strohle (1996), Active post-depositional oxidation of the most recent sapropel (S1) in sediments of the eastern Mediterranean, *Geochim. Cosmochim. Acta*, *60*, 4007–4024, doi:10.1016/S0016-7037(96)00253-0.

Vergnaud-Grazzini, C., W. B. F. Ryan, and M. Bianca Cita (1977), Stable isotopic fractionation, climate change and episodic stagnation in the eastern Mediterranean during the late Quaternary, *Mar. Micropaleontol.*, *2*, 353–370, doi:10.1016/0377-8398(77)90017-2.

Weldeab, S., D. W. Lea, R. R. Schneider, and N. Andersen (2007), 155,000 years of West African monsoon and ocean thermal evolution, *Science*, *316*, 1303–1307, doi:10.1126/science.1140461.

Yu, J., H. Elderfield, M. Greaves, and J. Day (2007), Preferential dissolution of benthic foraminiferal calcite during laboratory reductive cleaning, *Geochem. Geophys. Geosyst.*, *8*, Q06016, doi:10.1029/2006GC001571.

G. J. De Lange, S. Ní Fhlaithearta, and G.-J. Reichart, Department of Earth Sciences–Geochemistry, Faculty of Geosciences, Utrecht University, PO Box 80.021,NL-3508 TA Utrecht, Netherlands. (shauna@geo.uu.nl)

C. Fontanier and F. J. Jorissen, Laboratory of Recent and Fossil Bio-Indicators, UPRES EA 2644, Angers University, 2 blvd. Lavoisier, F-49045 Angers CEDEX 01, France.

E. J. Rohling and J. Thomson, National Oceanography Centre, European Way, Southampton SO14 3ZH, UK.